OPV. His birth and developmental history were normal. He was hospitalized and his perianal abscess was treated with intravenous antibiotics and dissection of the abscess. Although his perianal abscess resolved, his high fever continued. His crying became weaker and he suddenly developed a flaccid paralysis of his extremities and trunk on day 5 of hospitalization. Brain and sagittal spinal magnetic resonance imaging (MRI) did not show any obvious abnormalities (an axial MRI view of the spine was not performed). A lumbar puncture was performed and the cerebrospinal fluid (CSF) showed 7 mononuclear cells/mm^3, 91 mg/dL protein, and 49 mg/dL glucose. He received i.v. γ-globulin therapy (2 g/kg/dose). The flaccid paralysis of his upper limbs and trunk improved on day 10, however paralysis of both lower limbs, but predominantly the right, continued. Right patellar and Achilles tendon reflexes were not detectable and left patellar and Achilles tendon reflexes were diminished. Plantar reflexes were absent. Sensory abnormalities were not detectable, and bladder and rectal dysfunction were not noted.

On day 45, his CSF showed 21 mononuclear cells/mm^3, 28 mg/dL protein, and 49 mg/dL glucose. Polymerase chain reaction (PCR) for adenovirus, enteroviruses and herpes simplex viruses in the CSF was negative. The neutralizing antibody titer for poliovirus in the CSF was also negative.

Table 1 Serum poliovirus-neutralizing antibody titer of the patient at 40 days and 10 months after the onset of illness

Virus type	40 days	10 months
PV type 1	1 : 16	<1 : 4
PV type 2	1 : 16	1 : 4
PV type 3	1 : 32	1 : 4

PV, poliovirus.

All biochemical tests were within normal limits. In the serum, neutralizing antibody titers for poliovirus type 1, 2, and 3 were 1 : 16, 1 : 16, and 1 : 32, respectively. Ten months after onset, the corresponding antibody titers were negative, 1 : 4, and 1 : 4, respectively (Table 1). Detailed investigation of his immune status showed no abnormalities, both at the time of admission and 10 months later. White blood cell, neutrophil and lymphocyte counts were 18 300, 12 900 and 4026 cells/μL, respectively, and

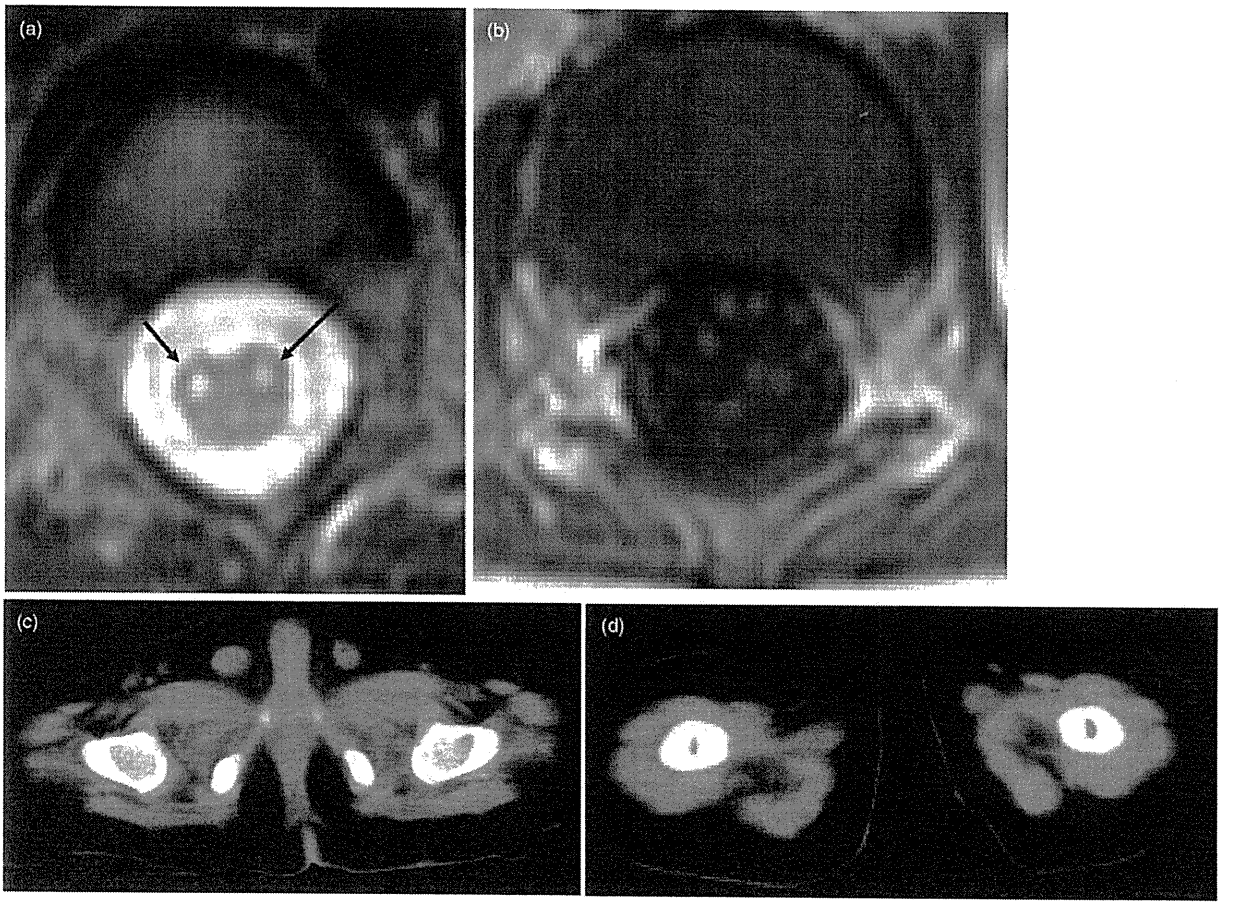

Fig. 1 Magnetic resonance imaging (MRI) and computed tomography (CT) images taken on day 39 of illness. (a) Axial image of T2-weighted MRI demonstrating bilateral high-intensity signals (arrows) in the anterior spinal cord at the level of T11. (b) Axial image of gadolinium-enhanced T1-weighted MRI demonstrating an enhanced ventral cauda equina. (c) CT images showing severe bilateral muscle atrophy in the gluteus and (d) femoral muscles.

his immunoglobulin (Ig) G level was 685 mg/dL at the time of admission. Ten months later, white blood cell, neutrophil and lymphocyte counts were 7400, 2146 and 4144 cells/μL, respectively; cluster of differentiation (CD)3-, CD4-, CD8-, CD19- and human leukocyte antigen (HLA)-DR-positive lymphocyte counts were 3037, 2076, 804, 820 and 887 cells/μL, respectively; and his IgG level was 806 mg/dL. Poliovirus was isolated from the feces on days 42 and 45 and was identified as poliovirus type 3 in a virus-neutralization test; it was later found to be a Sabin-3 (VP1 region)/Sabin-1 (3D region) recombinant vaccine strain because its serotype and intratypic differentiation were similar to OPV by the PCR-restriction fragment length polymorphism method and sequencing.[6]

T2-weighted MRI (axial section) on day 39 demonstrated a high-intensity signal bilaterally in the anterior horn of the spinal cord at the level of T11 and T12 (Fig. 1a). The sagittal view of the spinal MRI did not show any obvious abnormalities. Gadolinium-enhanced T1-weighted MRI showed an enhanced signal in the ventral cauda equina (Fig. 1b). Computed tomography on day 39 showed severe atrophy of the gluteus and femoral muscles bilaterally (Fig. 1c,d). Conduction velocities of the medial nerves were within normal limits, but conduction velocities of the tibial nerves were decreased (Fig. 2).

The infant underwent rehabilitation and physical therapy, but he still has severe motor impairment with hypotonia and weakness of the lower limbs at 2 years of age. He can stand using lower limb orthoses, but cannot walk; he also has severe scoliosis.

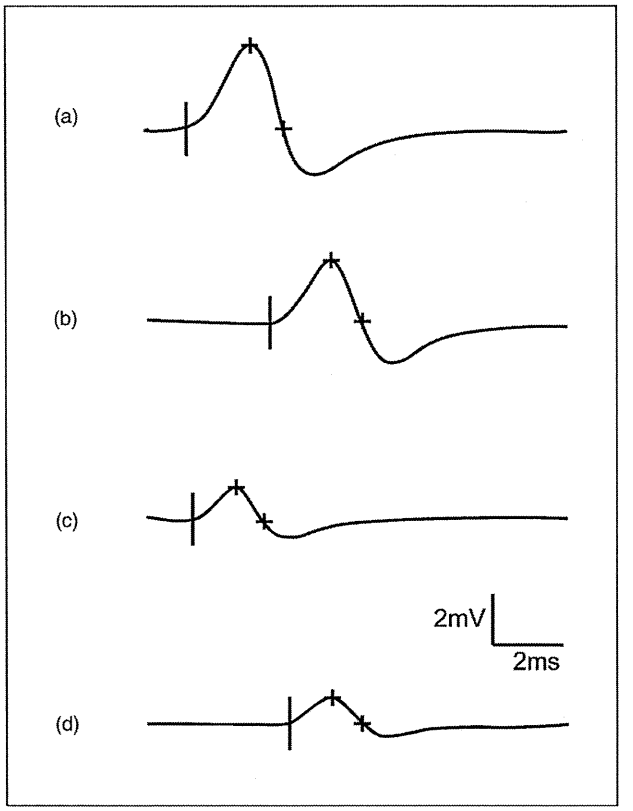

Fig. 2 Motor conduction velocities in the tibial nerve on day 40 of illness showing a reduction in the right side (left, 35.4 m/s; right, 28.5 m/s). (a) Left ankle stimulation; amplitude 4.3 mV. (b) Left knee stimulation; amplitude 3.2 mV. (c) Right ankle stimulation; amplitude 1.7 mV. (d) Right knee stimulation; amplitude 1.3 mV.

Discussion

Poliovirus is an enterovirus transmitted mainly by fecal-oral contamination. After poliovirus infection, most people are asymptomatic or have a non-specific illness including mild fever, malaise, headache, sore throat and gastrointestinal upset. Among those who have a non-specific illness, 1–2% of individuals progress to paralytic disease. The paralysis evolves and fixes rapidly during the fever, and often leaves asymmetrical muscle atrophy, but without sensory, bladder or rectal dysfunction. Although poliovirus can involve any structure of the nervous system, the virus tends to affect the larger motor neurons, particularly those of the anterior horn of the spinal cord and the motor nuclei of the medulla. In the acute to subacute phase, the ventral horn cells are characterized by a severe inflammation, neuronophagia, active gliosis and destruction of the anterior horn cells. This correlates with the abnormalities seen on spinal MRI.[7] In the present case, the abnormality could not be detected on the sagittal section of the spinal MRI, although the lesion existed in the anterior horn cells at the onset of paralysis.

Cases of VAPP have been reported in many countries using OPV.[2] In Japan and other countries VAPP is usually associated with polio virus type 2 and 3, but rarely type 1. The clinical course of VAPP is similar to that of wild poliovirus, so it is difficult to distinguish between VAPP and poliomyelitis caused by the wild virus. Previous reports indicate that persons with primary immunodeficiencies have a much higher risk of the disease.[3,4] The present case of recipient VAPP following the first OPV dose involved the type 3 vaccine virus, but we were unable to detect any obvious immunodeficiencies in the infant. We considered that his serum-neutralizing antibody titer for poliovirus on day 40 was raised under the influence of intravenous γ-globulin therapy besides vaccination. After ten months, his antibody titer for poliovirus type 2 and 3 had decreased, but was maintained at 1 : 4 and the immunity persisted. His antibody titer for poliovirus type 1 became negative after ten months suggesting that immunity was not acquired from a single vaccination.

Strebel *et al.*[8] reported that the risk of VAPP increased with tissue injury, such as intramuscular injection, within one month of immunization with OPV. It is also suggested that skeletal muscle injury induces retrograde axonal transport of poliovirus and thereby facilitates viral invasion of the central nervous system and progression of spinal cord damage.[9] Bosley *et al.*[10] reported an infant with VAPP who had a perianal abscess simultaneously. In our case, when the infant was given OPV, he might have had a perianal injury and he was treated for his perianal abscess just before his paralytic illness appeared. The perianal abscess itself, or dissection of the abscess, may have caused skeletal muscle injury and increased the risk of VAPP. We therefore consider that the perianal abscess was an important factor in the development of VAPP and influenced the pathogenesis of the disease.

It is apparent that VAPP occurs constantly in countries where the live virus polio vaccine is used, as adverse reactions to OPV in healthy infants without any obvious immunodeficiencies can occur, as in our case. In 2000, the American Academy of Pediatrics changed their policy to recommend only inactivated poliovirus vaccine (IPV) for routine childhood immunization, because they considered VAPP would not be eliminated unless the use of OPV was stopped.[11] Recently, some countries including the USA and Germany have changed their national policies to recommend vaccination with IPV alone instead of OPV.[12] Therefore, we believe that the introduction of IPV should be seriously considered in Japan.

References

1 Yoneyama T, Karoji Y, Watanabe K, Tsuchiya M, Nakano M, Miyamura T. Surveillance of poliovirus-isolates in Japan, 1999. *Jpn. J. Infect. Dis.* 2000; **53**: 90–1.

2 Global Commission for the Certification of the Eradication of Poliomyelitis. *Meeting (2002: Geneva, Switzerland). Report of the Interim Meeting of the Technical Consultative Group (TCG) on the Global Eradication of Poliomyelitis, Geneva, 13–14 November 2002*. World Health Organization, Geneva, 2003.

3 Parvaneh N, Shahmahmoudi S, Tabatabaie H *et al.* Vaccine-associated paralytic poliomyelitis in a patient with MHC class II deficiency. *J. Clin. Virol.* 2007; **39**: 145–8.

4 Manishi S, Shahmahmoudi S, Tabatabaie H *et al.* Novel *BTK* mutation presenting with vaccine-associated paralytic poliomyelitis. *Eur. J. Pediatr.* 2008; **167**: 1335–8.

5 Hao L, Toyokawa S, Kobayashi Y. Poisson-model analysis of the risk of vaccine-associated paralytic poliomyelitis in Japan between 1971 and 2000. *Jpn. J. Infect. Dis.* 2008; **61**: 100–3.

6 Balanant J, Guillot S, Candrea A, Delpeyroux F, Crainic R. The natural genomic variability of poliovirus analyzed by a restriction fragment length polymorphism assay. *Virology* 1991; **184**: 645–54.

7 Kornreich L, Dagan O, Grunebaum M. MRI in acute poliomyelitis. *Neuroradiology* 1996; **38**: 371–2.

8 Strebel PM, Ion-Nedelcu N, Baughman AL, Sutter RW, Cochi SL. Intramuscular injections within 30 days of immunization with oral poliovirus vaccine – a risk factor for vaccine associated paralytic poliomyelitis. *N. Engl. J. Med.* 1995; **332**: 500–6.

9 Gromeier M, Wimmer E. Mechanism of injury-provoked poliomyelitis. *J. Virol.* 1998; **72**: 5056–60.

10 Bosley AR, Speirs G, Markham NI. Provocation poliomyelitis: vaccine associated paralytic poliomyelitis related to a rectal abscess in an infant. *J. Infect.* 2003; **47**: 82–4.

11 American Academy of Pediatrics, Committee on Infectious Diseases. Prevention of poliomyelitis: recommendations for use of only inactivated poliovirus vaccine for routine immunization. *Pediatrics* 1999; **104**: 1404–6.

12 Alexander LN, Seward JF, Santibanez TA *et al.* Vaccine policy changes and epidemiology of poliomyelitis in the United States. *JAMA* 2004; **292**: 1696–701.

Conservative treatment of a large post-infectious pneumatocele

Leon Joseph,[1] Sarit Shahroor,[2] Drora Fisher,[3] Shmuel Goldberg[1] and Elie Picard[1]

[1]*Pediatric Pulmonology Unit,* [2]*Pediatric Intensive Care Unit,* [3]*Pediatric Radiology Department, Shaare Zedek Medical Center, Affiliated with the Hebrew University-Hadassah Medical School, Jerusalem, Israel*

Key words conservative management, necrotizing pneumonia, pneumatocele.

A pneumatocele (PC) is an air-filled cyst within the lung parenchyma that is usually thin-walled. It is most commonly seen in children secondary to a severe pulmonary infection sometimes complicated by pleural effusion.[1] The airways undergo necrosis and the resultant cystic lesion is connected to the bronchial tree. This connection is unidirectional causing hyperinflation of the cyst. In the past, the most common pathogen associated with PC was *Staphylococcus aureus*, but recently there has been an increase in the incidence of *Streptococcus-pneumoniae*-associated PC.[2,3] In two recent series of pneumococcal pneumonia, PC developed in 7%[2] and 18%[3] of the patients, respectively.

There is no fully accepted consensus for treatment of PC. In 1983, 12 cases of pneumatocele were reported with two patients who died from progressive respiratory failure with no apparent attempt to reduce the size of the PC.[4] In 1996, the first report of computed-tomography-(CT)-guided intrapulmonary drainage of five patients with PC had good results.[5] A recent paper by Imamoglu *et al.*[6] proposed a protocol for treating PC. According to their criteria, PC larger than 50% of the hemithorax, those that cause severe atelectasis, those that have persistent symptoms, or are poorly tolerated during follow up, should be treated. Using "thin wall" as another indication for treatment, they recommend image-(CT)-guided catheter drainage (IGCD) as having good results in their series for all those drained who had thin-walled PC. However, two cases in their series that had long-standing thick-walled PC were not cured after catheter drainage and underwent surgical resection.

Although our case fulfilled the above criteria for drainage, it was successfully treated conservatively. Our Institutional Review Board waived the need for consent.

Correspondence: Elie Picard, MD, Pediatric Respiratory Unit, Shaare Zedek Medical Center, Jerusalem 91031, Israel. Email: picard@szmc.org.il

Received 19 November 2009; revised n/a; accepted 1 February 2010.

doi: 10.1111/j.1442-200X.2010.03137.x

Case Report

A 14-month-old male infant presented to our emergency department with fever and cough. A full examination and blood count

MERRF/MELAS overlap syndrome: a double pathogenic mutation in mitochondrial tRNA genes

M Nakamura,[1] I Yabe,[1] A Sudo,[2] K Hosoki,[2] H Yaguchi,[1] S Saitoh,[2] H Sasaki[1]

[1]Department of Neurology, Hokkaido University Graduate School of Medicine, Sapporo, Japan
[2]Department of Pediatrics, Hokkaido University Graduate School of Medicine, Sapporo, Japan

Correspondence to
Ichiro Yabe, Department of Neurology, Hokkaido University Graduate School of Medicine, N15W7, Kita-ku, Sapporo 060-8638, Japan;
yabe@med.hokudai.ac.jp

MN & IY contributed equally to this study.

Received 31 October 2009
Accepted 11 January 2010
Published Online First
7 July 2010

ABSTRACT

Background Myoclonic epilepsy with ragged-red fibres (MERRF) and mitochondrial encephalopathy, lactic acidosis and stroke-like episodes (MELAS) are established phenotypes of mitochondrial encephalomyopathy. The m.8356T>C transition in the mitochondrial $tRNA^{Lys}$ gene is a pathogenic mutations of MERRF. The m.3243A>G transition in the mitochondrial $tRNA^{Leu}$ gene is detected in most MELAS patients. Although previous analyses of double mutations in mitochondrial DNA (mtDNA) were useful for discussing their nature, many unsolved questions remain.

Objective To describe the clinical and genetic features of a family with the above mtDNA double-point mutations and discuss the role of double mtDNA mutations in diverse clinical features in the family.

Patients and methods The proband was a 23-year-old woman with MERRF harbouring m.8356T>C and m.3243A>G transitions in mitochondrial tRNA genes. We assessed clinical aspects of her and those of her three relatives and performed mutation analyses on their mtDNA.

Results Phenotypes of the four patients were MERRF, MERRF/MELAS overlap syndrome and asymptomatic carrier. We hypothesise that the course of the phenotype of this family begins with MERRF and is followed by MELAS. This double mutation was heteroplasmic in blood of all four patients but with different rates in each patient, while m.8356T>C appeared homoplasmic and m.3243A>G was heteroplasmic in muscle of the two examined cases. No other mutations were detected in the total mtDNA sequence in this family.

Conclusions This is the first reported case of a double-point mutation in mtDNA, both of which were heteroplasmic and pathogenic for the established phenotypes.

The concept of myoclonic epilepsy with ragged-red fibres (MERRF) was first proposed in 1980 and has been established as one of the phenotypes of mitochondrial encephalomyopathy.[1] It is maternally inherited, and patients express myoclonus, myoclonic or generalised convulsions, cerebellar ataxia and myopathy with ragged-red fibres.[2] In 1990, the most common pathogenic mutation, m.8344A>G transition, in the mitochondrial $tRNA^{Lys}$ gene was reported,[3] and report of a second pathogenic mutation, m.8356T>C transition, in the mitochondrial $tRNA^{Lys}$ gene followed in 1992.[4] The first report of the m.8356T>C transition indicated a pure MERRF expression[4]; however, subsequent reports revealed that patients, with or without MERRF symptoms, of the families with this mutation, frequently showed migraine, stroke-like episodes and strongly succinate dehygrogenase-reactive vessels (SSVs) in muscle pathology, which are typical for another phenotype of mitochondrial encephalomyopathy; mitochondrial myopathy, encephalopathy, lactic acidosis and stroke-like episodes (MELAS).[5 6] It was speculated that the m.8356T>C transition might occur in patients with some of the expressions of MELAS, such as migraine, stroke-like episodes and SSVs; however, the mechanism by which various expressions typical for two distinct phenotypes might occur in patients with only this point mutation in mitochondrial DNA (mtDNA) has not been clarified.[5 6]

The concept of MELAS was proposed in 1984, also as one of the phenotypes of mitochondrial encephalomyopathy.[7] This entity was maternally inherited and characterised by stroke-like episodes, episodic headache and vomiting, seizures, dementia, lactic acidosis, skeletal myopathy, short stature and as being with or without MERRF symptoms.[7] The first pathogenic mutation, the m.3243A>G transition in the mitochondrial $tRNA^{Leu}$ gene, was reported in 1990.[8] Moreover, it was revealed that most of the patients with MELAS had this mutation as a primary cause of the disease.[9] On the other hand, there were several reports of patients with an m.3243A>G transition, who also expressed features typical of phenotypes of mitochondrial encephalmyopathy other than MELAS, such as MERRF,[10 11] MERRF/MELAS overlap syndrome,[12 13] progressive external ophthalmoplegia (PEO) and MERRF/PEO overlap syndrome,[14] suggesting that the m.3243A>G transition was potentially indicative of a broad expressive spectrum. However, what determined the range of expression in each patient had not been resolved.[10–14]

There are reports of rare families with mitochondrial encephalomyopathy, possessing double-point mutations in mtDNA.[15–22] Some of these consist of two mutations reported to separately express the same[15 18 20 22] or different[17 19 21] distinct phenotypes, and others consist of one mutation of a well-known pathogenesis and one mutation of unknown effect.[16] It is speculated that in some families, only one of the mutations expresses a phenotype,[16 17] that each mutation expresses different phenotypes in a given family[19] and both mutations act synergistically to express one phenotype in other families.[18 21 22] These double mtDNA mutations might be the key to resolving the mechanisms underlying the formation of threshold effects. However, these issues have yet to be resolved, presumably due in part to the various combinations of established phenotypes and mutational expressions in each of the families mentioned above.

We encountered a family with the double mutation, m.8356T>C and m.3243A>G. Individual family members expressed MERRF, MERRF/MELAS overlap syndrome and other minor complications compatible with symptoms derived from mitochondrial dysfunctions. Because the various family members express potential phenotypes known to be caused by these two mtDNA mutations, they were considered advantageous for discussing the relationship between phenotypes and genetic effects. We had a chance to examine four members of this family and tried to clarify the expression and the role of mtDNA point mutations.

PATIENTS AND METHODS

Patients

The pedigree of the family we will discuss is shown in figure 1. We first met patient III-1 (proband). She was introduced to us from another institution, diagnosed with myoclonic epilepsy. An interview of her and her mother (II-1) revealed that they had a familial history of mitochondrial encephalomyopathy (II-2; maternal aunt of the proband). We subsequently discovered that one of our colleagues had examined II-2 and had identified mtDNA double-point mutation (m.8356T>C and m.3243A>G) by a commercial-based (SRL Inc.) analysis of common mtDNA mutations and that her muscle specimen had been preserved in our institution. Another patient of this family (III-6; cousin of the proband) was introduced to us from another institution, also diagnosed with myoclonic epilepsy. Thus, the main participants of this study are these four cases: II-1 (mother), II-2 (maternal aunt), III-1 (proband) and III-6 (cousin). This pedigree contains other cases with hearing loss (I-1), hearing loss and mental retardation (III-5) and sudden death at one year of age (III-7). However, as we did not encounter these family members, we have no further information about them.

We conducted clinical (physical, neurological, laboratory and radiological) examinations of II-1, III-1 and III-6 as far as we could. Clinical information of II-2 was gained from medical records. Histochemical analysis of muscle was conducted for II-2 and III-1. Genetic analyses of mtDNA from blood and/or muscle was conducted in all four cases.

Report of cases

III-1: the proband

A 17-year-old woman with bilateral sensorineural deafness developed a generalised clonic convulsion; she was diagnosed with myoclonic epilepsy 1 year later. Sodium valproate had been effective for preventing relapses of epileptic seizures. She was introduced to us at age 23 because her maternal aunt (II-2) was diagnosed with MELAS. She exhibited a slightly short stature (154 cm) and definitely low body weight (36 kg). She did not complain of either episodic headache or nausea. Neurological examinations revealed deafness, slurred speech, weakness of bilateral quadriceps, and limb and truncal ataxia. By conversation, we were impressed that although she was somewhat childish for her age, her cognitive function was preserved. Her visual acuity and field were not disturbed. External ophthalmoplegia was not observed. Serum chemistry examinations detected no elevations in lactate, creatine kinase, transaminases, lactate dehydrogenase, amylase, haemoglobin A_{1c} and creatinine. Blood hormonal evaluations of pituitary gland (ACTH, TSH, LH, FSH, GH, and prolactin), thyroid (fT3, fT4), adrenal cortex (cortisol) and genitals (oestradiol) were normal. Elevated lactate was detected in cerebrospinal fluid (35.3 mg/dl; normal<20.0 mg/dl). A CT scan of the trunk showed no abnormal forms of the organs in chest and abdomen. Transthoracic ultrasonic cardiography did not reveal cardiomyopathy. A brain MRI scan showed diffuse mild brain atrophy without focal lesions. Electroencephalography (EEG) showed bilateral slow waves. A muscle biopsy of the left *rectus femoris* revealed fibre size variability, scattered ragged-red fibres (RRFs) and SSVs (figure 2A). Cytochrome c oxidase defects were detected in occasional fibres (focal COX deficiency), also among RRFs (figure 2B). Most of the SSVs (approximately 80%) possessed COX activity.

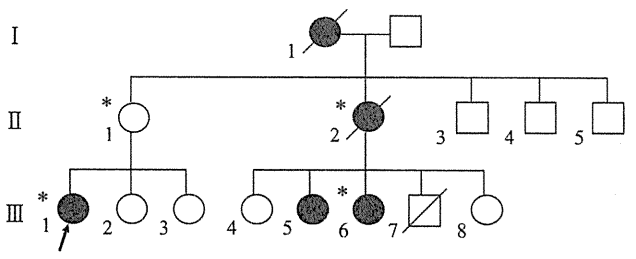

Figure 1 Proband's family pedigree. ○=woman; □=man; /=deceased. Solid symbols are symptomatic members. The arrow shows the proband. * Patients we encountered.

II-2: maternal aunt of III-1

The proband's maternal aunt had bilateral sensorineural deafness and progressive myoclonic epilepsy when she was 26 years old. At age 38, she developed stroke-like episodes with headache, truncal instability and convulsion; she exhibited emaciation (stature 157 cm, body weight 38 kg). Neurological examinations revealed aphasia, right hemianopsia and cerebellar ataxia. A brain MRI scan showed a large lesion in the left cerebral hemisphere (figure 3). Elevated lactate (34.6 mg/dl; normal <16.0 mg/dl) and impaired glucose tolerance (data not shown) were detected in serum. A muscle biopsy of the left *rectus femoris* showed fibre size variability, RRFs, focal COX deficiency and SSVs (figure 2C,E). Some SSVs (approximately 40%) lacked COX activity (figure 2C–F), and occasional RRFs also lacked COX activities. A stroke-like episode relapsed with disturbed consciousness at age 45, and the patient died of renal and heart failure 1 year later.

III-6: cousin of III-1

A female cousin of the proband developed slurred speech, dysmetria of all four extremities and truncal instability at age 18. After a few months, myoclonic jerks of the upper extremities often appeared, followed by generalised clonic convulsions. Her stature and body weight were in the normal range. She had neither deafness nor a history of episodic headache and nausea. Neurological findings revealed a slight cerebellar ataxia of the trunk and limbs, transient myoclonus of the upper extremities and an episode of generalised convulsion. She appeared childish during conversation, but intellectual ability was normal. Her visual acuity and field were intact. External ophthalmoplegia was not observed. Serum creatine kinase, transaminases, lactate dehydrogenase, amylase, haemoglobin A_{1c} and creatinine were within normal limits, but lactate was elevated (16.4 mg/dl; normal<16.0 mg/dl). Transthoracic ultrasonic cardiography indicated normal wall motion of the heart. A brain MRI showed no definite abnormalities. She showed left dominant spike-and-waves on an EEG and was diagnosed with myoclonic epilepsy at age 19. For about 1.5 years, myoclonic epilepsy was well controlled with carbamazepine; however, at age 21, the frequency of the epileptic seizures increased. Despite changes to,

J Med Genet 2010;**47**:659–664. doi:10.1136/jmg.2009.072058

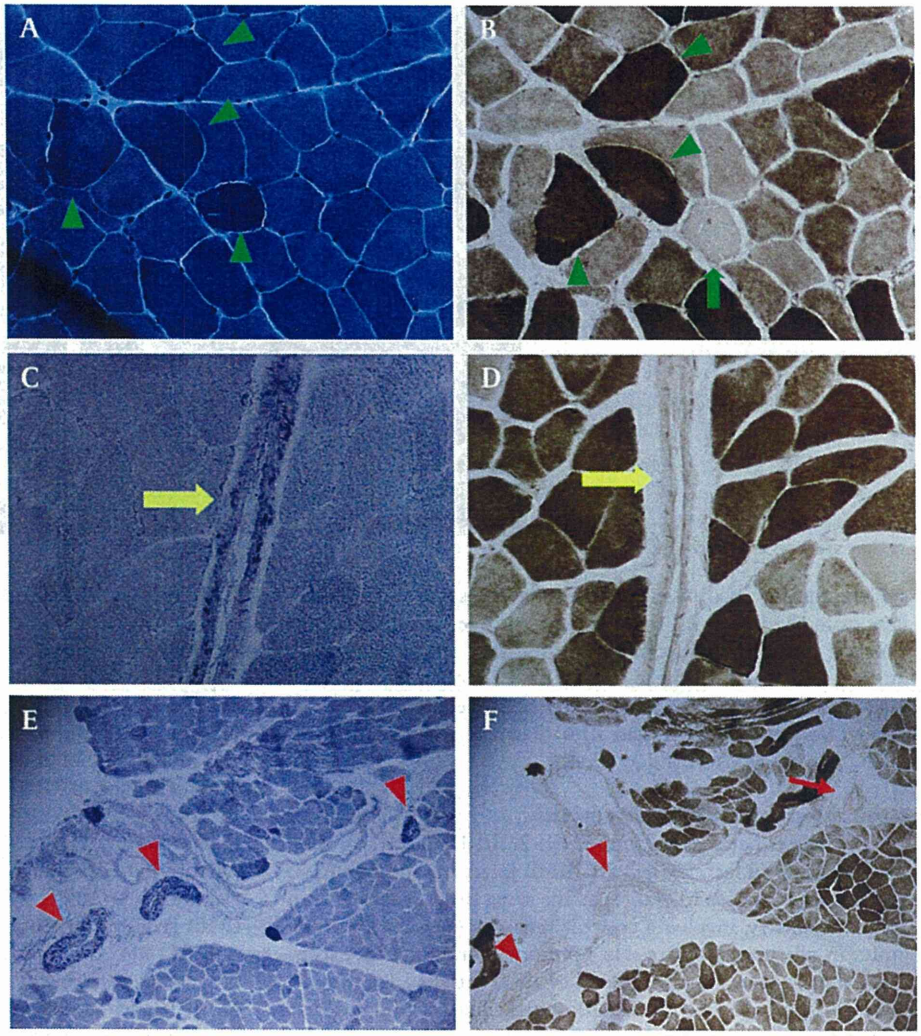

Figure 2 Pathology observed in *rectus femoris* muscle biopsies in III-1 (A and B) and II-2 (C, D, E and F). A and B, C and D, and E and F are pairs of adjacent sections stained as indicated. (A) Scattered ragged-red fibers (RRFs). Modified Gomori trichrome stain, ×400. (B) Occasional RRFs with (arrowheads) or without (arrow) cytochrome c oxidase (COX) activities. COX stain, ×400. (C) Strongly succinate dehydrogenase-reactive blood vessels (SSVs) (arrow). Succinate dehydrogenase (SDH) stain, ×400. D; SSVs with COX activities (arrow). COX stain, ×400. (E) SSVs (arrowheads). SDH stain, ×100. (F) SSVs without COX activities (arrowheads) and with mild COX activities (arrow). COX stain, ×100.

or additions of, other antiepileptic drugs (phenytoin, zonisamide, topiramate, sodium valproate), control of seizures was difficult, and she required intensive care with mechanical ventilation twice during status epilepticus (SE). Moreover, in the course of treatment for the second SE, abdominal pain and elevated serum amylase and lipase occurred. A CT scan and an ultrasonogram detected no abnormal changes in the pancreas. Following treatment with camostat mesilate, ursodeoxycholic acid and ulinastatin, the symptoms were relieved and serum pancreatic enzymes were normalised in 1 month.

II-1: mother of III-1

The proband's mother, at age 51, was asymptomatic.

mtDNA mutation analysis

The examination of mtDNA mutations was first conducted in II-2 at another institution. She appeared to express the features of both MERRF and MELAS. Therefore, two established pathogenic mutations in mtDNA found in these phenotypes, m.8356T>C and m.3243G>A, were selected and screened for using commercial-based analyses of blood (SRL Inc.); both point mutations were found. Therefore, we also screened for these mtDNA mutations in blood and muscle of III-1 and in the preserved muscle specimen of II-2. The m.8356T>C and m.3243A>G mutations were detected by PCR-restriction fragment length polymorphism analysis. Genomic DNA was extracted from blood and muscle specimens and amplified by PCR. PCR primers for m.3243A>G were adopted from Goto *et al*,[8] while mismatch primers to detect m.8356T>C substitution were adopted from Silvesti *et al*.[4] PCR products were digested with *Apa*I and *Dra*I at positions 3243 and 8356, respectively. Plasmids containing only wild-type or mutant mtDNA were constructed and used as controls. PCR products were also sequenced to confirm the base substitutions. Blood samples of two other family members whom we had chances to examine (II-1 and III-6) were also analysed with the same procedure. Moreover, whole mtDNA genome analyses in blood and muscle of III-1 and in blood of II-1 were conducted (mitoSEQr resequencing system, for resequencing the entire mitochondrial genome with 46 RSAs. Applied Biosystems, USA).

RESULTS

Symptoms and phenotypes

The phenotypes of the proband (III-1) and cousin (III-6) were MERRF, the aunt (II-2) was MERRF/MELAS overlap syndrome and the mother (II-1) was an asymptomatic carrier. Three other members (I-1, III-5 and III-7) also had some symptoms that could not be categorised in distinct entities. Of the three patients with MERRF (III-1 and III-6) and MERRF/MELAS overlap syndrome (II-2), two (II-2 and III-1) showed short

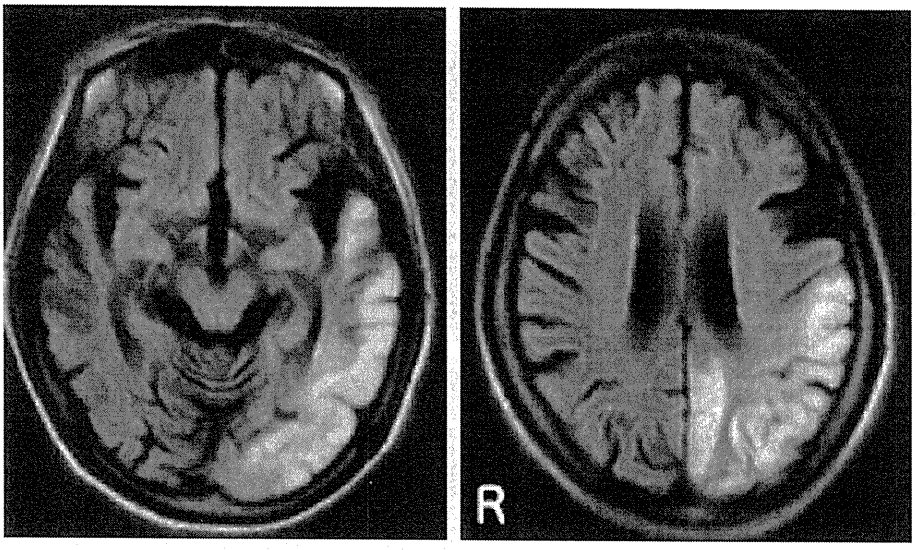

Figure 3 Brain MRI of II-2 during acute phase. FLAIR images detected a hyperintense lesion extending from the left occipito-parieto-temporal lobe at 38 years. R: right.

stature and low body weight with bilateral sensorineural deafness from childhood. All three patients suffered from myoclonic epilepsy from the late teens to the mid-20s. Patient II-2 subsequently exhibited episodic headache in her mid-30s, with a stroke-like episode that repeatedly occurred afterwards. The other two patients (III-1 and III-6) had not reached their 30s when this study was conducted.

Blood and cerebrospinal fluid analysis

Of the three patients examined (II-2, III-1 and III-6), two showed elevated lactate (II-2 and III-6) in serum and one (II-2) had impaired glucose tolerance; at the same time, other items in serum chemistry, involving creatine kinase, were within normal limits in all three patients. No hormonal abnormalities except short stature were found in blood of III-1. Patient III-1 showed high levels of lactate in cerebrospinal fluid (CSF was not examined in the other patients).

Radiological examinations and EEG findings

Of the three patients examined, brain MRIs in two of them (II-2 and III-1) showed diffuse brain atrophy, with stroke-like lesions in II-2, while patient III-6 exhibited a normal brain MRI. Transthoracic ultrasonic cardiographies demonstrated normal cardiac wall motion in the two patients examined (III-1 and III-6). Thoracic and abdominal CT scans detected no abnormalities in III-1. Two patients (III-1 and III-6) underwent EEG. III-1 showed generalised slow waves, and III-6 exhibited focal spike-and-waves.

Muscle pathology

Muscle biopsies were conducted in two cases (II-2 and III-1). II-2 had already expressed stroke-like episodes at the time this procedure was conducted. The two patients had similar morphological findings: fibre size variability, RRFs, focal COX deficiency, SSVs and a mosaic distribution of COX activities in both RRFs and SSVs (figure 2). The proportion of the SSVs with COX deficiencies was higher in III-1 than in II-2.

Genetic analysis

Results of genetic analyses are shown in figure 4. Genetic analysis of mtDNA in III-1 revealed heteroplasmic m.8356T>C and m.3243A>G mutations in blood. This double mtDNA mutation was also detected and was heteroplasmic in the blood of II-1 and III-6, although the proportions of both mutations were clearly less in asymptomatic II-1. In muscle of III-1, the proportion of m.3243A>G was higher than that in blood and m.8356T>C appeared to be homoplasmic. In muscle of II-2, m.3243A>G was heteroplasmic and m.8356T>C also appeared to be homoplasmic. Screening of the entire mtDNA genomes from blood and muscle of III-1 and from blood of II-1 revealed no mutations other than the m.8356T>C and m.3243G>A transitions.

Discussion

All four patients that we encountered carried the double-point mutations m.8356T>C and m.3243A>G in mitochondrial tRNA genes. Both mutations were heteroplasmic in blood, while m.8356T>C appeared to be homoplasmic in muscle. The proportion of m.3243A>G transitions was higher in the muscle of III-1 and seemed to be associated with clinical severity because all symptomatic patients had significant proportions of the mutation, but the asymptomatic patient II-1 carried the lowest mutational load. The m.8356T>C mutation appeared to be homoplasmic in muscle of III-1 and II-2, although a low level

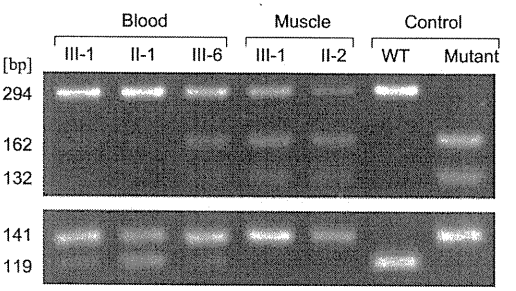

Figure 4 Restriction fragment length polymorphism analysis for the m.3243A>G and m.8356T>C mutations. Upper panel demonstrates variable heteroplasmy level of the m.3243A>G mutation in the pedigree. Uncut 294 bp band represents the wild type (3243A) while the 162 and 132 bp bands represent the mutant (3243G). Ratio of the mutant in muscle is significantly higher than in blood of III-1. Lower panel also shows variable heteroplasmy level of the m.8356T>C mutation. Uncut 141 bp band represents the mutant (8356C) while the 119 and 22 bp bands (only the 119 bp band is shown) represent the wild-type (8356T). The mutation rate in muscle is higher than in blood and appears to be homoplasmic in III-1 and II-2. WT and Mutant represent cloned plasmid DNAs containing only wild-type and mutation sequences, respectively.

J Med Genet 2010;**47**:659–664. doi:10.1136/jmg.2009.072058

of heteroplasmy cannot be excluded due to the limitation of our current semi-quantitative PCR analysis. Nevertheless, it is fair to say that the m.8356T>C transition was higher in muscle than in blood, at least in III-1. The proportion of m.8356T>C transitions also appeared to be associated with clinical severity.

The four patients showed phenotypes of MERRF (III-1 and III-6), MERRF/MELAS overlap syndrome (II-2) and of an asymptomatic carrier (II-1). There were several other symptomatic family members (I-1, III-5 and III-7). We suggest that the typical course of disease in this family is as follows: the onset is characterised by short stature with emaciation and bilateral sensorineural deafness in childhood followed by cerebellar ataxia and myoclonic epilepsy; MERRF expression follows in young adulthood. By middle age, the disease progression is characterised by the addition of migraine, vomiting and stroke-like episodes, symptoms of MELAS expression that indicate completion of the MERRF/MELAS overlap syndrome. Muscle pathology is compatible with MELAS before and after phenotypic expression of MELAS.[9 23] However, a quantitative association between SSVs with COX deficiencies and expression of MELAS was not found in this study. This might mean that these family members gain the potential to express MELAS from the mutation loads in their primary phases. The characteristic brain MRI and EEG findings were not observed in this family. Neither were external ophthalmoplegia nor cardiomyopathy detected.

We presume that these mutations are pathogenic for the observed clinical phenotypes based on the following criteria; (1) m.8356T>C and m.3243A>G transitions are pathogenic for MERRF[5 6] and MELAS,[8] respectively; (2) both mutations were heteroplasmic in blood of all four cases; (3) no mutations other than m.8356T>C and m.3243A>G were detected in total sequences of mtDNA from blood of II-1 or from blood and muscle of III-1; (4) other symptomatic members of the pedigree had symptoms indicative of mitochondrial dysfunction.[2]

Patients with the m.8356T>C transition frequently express both MERRF and MELAS.[5 6] Moreover, some patients with the m.3243A>G transition exhibit MERRF[10 11] or MERRF/MELAS overlap syndrome.[12 13] As we did not quantitatively evaluate these mutations or clarify their thresholds, we were unable to determine whether both mutations simultaneously affected the observed clinical phenotypes.

In II-2, with MERRF/MELAS overlap syndrome, MERRF preceded MELAS. In the next generation, the proband (III-1) expressed MERRF without MELAS. However, her muscle pathology showed RRFs and SSVs with COX activities, which are more characteristic of MELAS than MERRF,[23] and SSVs might be a predictor of stroke-like episodes[24] and additional MELAS expression. This finding leads us to speculate that the m.3243A>G transition might be pathogenic for expressing MELAS. Because the proportion of another mtDNA point mutation in muscle (m.12320A>G) was shown to increase overtime,[25] we hypothesise that the possibly increasing m.8356T>C transitions in our family might first overcome the threshold for the biochemical and symptomatic expressions of MERRF, and the increasing m.3243A>G transitions might then finally reach the threshold of symptomatic MELAS expression. It is presumed that neither mutation had reached its threshold in the asymptomatic family members. However, to demonstrate the pathogenicity of the m.3243A>G transition in the expression of MELAS, single-muscle fibre studies and more precise mtDNA species analyses are required. Without these data, it remains unknown whether a stroke-like episode of patient II-2 may be ascribed to m.3243A>G, because the m.8356T>C mutation itself can lead to the expression of MELAS/MERRF overlap syndrome.[5 6] Among further studies that we are planning, the screening for m.3243A>G transitions in urinary sediment samples will also be informative for determining clinical severity. Data have shown that assessment of mtDNA mutational load in urinary cells correlates closely with that observed in skeletal muscle[26 27] and is also a reliable measure of clinical severity.[28]

Most of the reported cases of patients with more than one mtDNA mutation carried double-point mutations[15–22]; however, cases with two heteroplasmic mtDNA point mutations were observed by Bidooki *et al* in only one family with m.10010T>C and m.5656A>G transitions in the $tRNA^{Gly}$ gene and in the non-coding region between the $tRNA^{Asn}$ and $tRNA^{Aln}$ genes, respectively.[16] The former mutation was pathogenic, while the latter was silent, and the associated phenotypes have not been generally established even in the former.[16] By contrast, both of the mutations in our family are known to express established phenotypes. The difference between this work and the 1997 publication by Bidooki *et al*[16] is that in the current study, there are potentially two pathogenic mtDNA mutations rather than a pathogenic mutation and a SNP. However, the causal effects must be investigated experimentally.

There are, as yet, no reports of double mtDNA mutations in which no evolutionary associations with one another were shown.[15–22] Thus, we presume that some of the double mutations in our family were in the same mitochondria and some occurred as single mutations in distinct mitochondria. If further studies demonstrate this condition (ie, the recombination of mtDNA[16] and one mutation's effect arising along with another in mtDNA[29]), single muscle fibre analysis and quantitative evaluations of the heteroplasmic rate of both mutations in each tissue might provide more profound insights into mtDNA mutations.

Main messages

- This is the first reported case of a double point mutation (m.8356T>C and m.3243A>G) in mitochondrial DNA (mtDNA), both of which were heteroplasmic and pathogenic for the mitochondrial encephalomyopathy phenotypes of myoclonic epilepsy with ragged-red fibers (MERRF) and mitochondrial encephalopathy, lactic acidosis, and stroke-like episodes (MELAS).
- Phenotypes of the four patients in this family were MERRF, MERRF/MELAS overlap syndrome, and asymptomatic carrier.
- All four patients carried double point mutations, m.8356T>C and m.3243A>G transitions, in mitochondrial tRNA genes. Both mutations were heteroplasmic in blood, while m.8356T>C appeared to be homoplasmic in muscle.

Current research questions

- Further studies will demonstrate this condition (ie, the recombination of mtDNA and one mutation's effect arising along with another in mtDNA). Single muscle fiber analysis and quantitative evaluations of the heteroplasmic rate of both mutations in each tissue might provide more profound insights into mtDNA mutations.

Acknowledgements We thank all patients for their active cooperation. This work was supported in part by a Grant-in-Aid for Scientific Research from the Ministry of Education, Science, Sports and Culture, Japan and by a grant from the Uehara Foundation.

Competing interests None.

Patient consent Obtained.

Ethics approval This study was conducted with the approval of the Hokkaido University Ethics Committee.

Provenance and peer review Not commissioned; externally peer reviewed.

REFERENCES

1. **Fukuhara N,** Tokiguchi S, Shirakawa K, Tsubaki T. Myoclonus epilepsy associated with ragged-red fibers (mitochondrial abnormalities): disease entity or a syndrome? *J Neurol Sci* 1980;**47**:117–33.
2. **DiMauro S,** Moraes CT. Mitochondrial encephalomyopathies. *Arch Neurol* 1993;**50**:1197–208.
3. **Shoffner JM,** Lott MT, Lezza AM, Seibel P, Ballinger SW, Wallace DC. Myoclonic epilepsy and ragged-red fibers (MERRF) is associated with a mitochondrial DNA $tRNA^{Lys}$ mutation. *Cell* 1990;**61**:931–7.
4. **Silvesti G,** Moraes CT, Shanske S, Oh SJ, DiMauro S. A new mtDNA mutation in the RNA^{LYS} gene associated with myoclonus epilepsy and ragged-red fibers (MERRF). *Am J Hum Genet* 1992;**51**:1213–7.
5. **Sano M,** Ozawa M, Shiota S, Momose Y, Uchigata M, Goto Y. The $T\text{-}C^{(8356)}$ mitochondrial DNA mutation in a Japanese family. *J Neurol* 1996;**243**:441–4.
6. **Zeviani M,** Muntoni F, Savarese N, Serra G, Tiranti V, Carrara F, Mariotti C, DiDonato S. A MERRF/MELAS overlap syndrome associated with a new point mutation in the mitochondrial DNA $tRNA^{Lys}$ gene. *Eur J Hum Genet* 1993;**1**:80–7.
7. **Pavlakis SG,** Phillips PC, DiMauro S, De Vivo DC, Rowland LP. Mitochondrial myopathy, encephalopathy, lactic acidosis, and stroke like episodes: a distinctive clinical syndrome. *Ann Neurol* 1984;**16**:481–8.
8. **Goto Y,** Nonaka I, Horai S. A mutation in the $tRNA^{LEU\ (UUR)}$ gene associated with the MELAS subgroup of mitochondrial encephalomyopathies. *Nature* 1990;**348**:651–3.
9. **Goto Y.** Clinical features of MELAS and mitochondrial DNA mutations. *Muscle Nerve* 1995;**3**:107–12.
10. **Folgero T,** Torbergsen T, Oian P. The 3243 MELAS mutation in a pedigree with MERRF. *Eur Neurol* 1995;**35**:168–71.
11. **Fabrizi GM,** Cardaioli E, Grieco GS, Cavallaro T, Malandrini A, Manneschi L, Dotti MT, Federico A, Guazzi G. The A to G transition at nt 3243 of the mitochondrial (RNALeu(UUR)) may cause a MERRF syndrome. *J Neurol Neurosurg Psychiatr* 1996;**61**:47–51.
12. **Campos Y,** Martin MA, Lorenzo G, Aparicio M, Cabello A, Arenas J. Sporadic MERRF/MELAS associated with the 3243 $tRNA^{LEU\ (UUR)}$ mutation of mitochondrial DNA. *Muscle Nerve* 1996;**19**:187–90.
13. **Mongini T,** Doriguzzi C, Chiadò-Piat L, Silvestri G, Servidei S, Palmucci L. MERRF/MELAS overlap syndrome in a family with A3243G mtDNA mutation. *Clin Neuropathol* 2002;**21**:72–6.
14. **Verma A,** Moraes CT, Shebert RT, Bradley WG. A MERRF/PEO overlap syndrome associated with the mitochondrial DNA 3243 mutation. *Neurology* 1996;**46**:1334–6.
15. **Riordan-Eva P,** Sanders MD, Govan GG, Sweeney MG, Da Costa J, Harding AE. The clinical features of Leber's hereditary optic neuropathy defined by the presence of a pathogenic mitochondrial DNA mutation. *Brain* 1995;**118**:319–37.
16. **Bidooki SK,** Johnson MA, Chrzanowska-Lightowlers Z, Bindoff LA, Lightowlers RN. Intracellular mitochondrial triplasmy in a patient with two heteroplasmic base changes. *Am J Hum Genet* 1997;**60**:1430–8.
17. **Arenas J,** Campos Y, Bornstein B, Ribacoba R, Martín MA, Rubio JC, Santorelli FM, Zeviani M, DiMauro S, Garesse R. A double mutation (A8296G and G8363A) in the mitochondrial DNA $tRNA^{Lys}$ gene associated with myoclonus epilepsy with ragged-red fibers. *Neurology* 1999;**52**:377–82.
18. **Brown MD,** Allen JC, Van Stavern GP, Newman NJ, Wallace DC. Clinical, genetic, and biochemical characterization of a Leber hereditary optic neuropathy family containing both the 11778 and 14484 primary mutations. *Am J Med Genet* 2001;**104**:331–8.
19. **Mimaki M,** Ikota A, Sato A, Komaki H, Akanuma J, Nonaka I, Goto Y. A double mutation (G11778A and G12192A) in mitochondrial DNA associated with Leber's hereditary optic neuropathy and cardiomyopathy. *J Hum Genet* 2003;**48**:47–50.
20. **Tonska K,** Kurzawa M, Ambroziak AM, Korwin-Rujna M, Szaflik JP, Grabowska E, Szaflik J, Bartnik E. A family with 3460G>A and 11778G>A mutations and haplogroup analysis of Polish Leber hereditary optic neuropathy patients. *Mitochondrion* 2008;**8**:383–8.
21. **Dai D,** Lu Y, Chen Z, Wei Q, Cao X, Xing G. Co-segregation of the T1095C with the A1555G mutation of the mitochondrial 12S rRNA gene in a patient with non-syndromic hearing loss. *Biochem Biophys Res Commun* 2008;**377**:1152–5.
22. **Zhang AM,** Jia X, Yao YG, Zhang Q. Co-occurrence of A1555G and G11778A in a Chinese family with high penetrance of Leber's hereditary optic neuropathy. *Biochem Biophys Res Commun* 2008;**376**:221–4.
23. **Goto Y,** Horai S, Matsuoka T, Koga Y, Nihei K, Kobayashi M, Nonaka I. Mitochondrial myopathy, lactic acidosis, and stroke-like episodes (MELAS): a correlative study of the clinical features and mitochondrial DNA mutation. *Neurology* 1992;**42**:545–50.
24. **Hasegawa H,** Matsuoka T, Goto Y, Nonaka I. Strongly succinate dehydrogenase-reactive blood vessels in muscles from patients with mitochondrial myopathy, encephalopathy, lactic acidosis, and stroke-like episodes. *Ann Neurol* 1991;**29**:601–5.
25. **Weber K,** Wilson JN, Taylor L, Brierley E, Johnson MA, Turnbull DM, Bindoff LA. A new mtDNA mutation showing accumulation with time and restriction to skeletal muscle. *Am J Hum Genet* 1997;**60**:373–80.
26. **McDonnell MT,** Schaefer AM, Blakely EL, McFarland R, Chinnery PF, Turnbull DM, Taylor RW. Noninvasive diagnosis of the 3243A>G mitochondrial DNA mutation using urinary epithelial cells. *Eur J Hum Genet* 2004;**12**:778–81.
27. **Shanke S,** Pancrudo J, Kaufmann P, Engelstad K, Jhung S, Lu J, Naini A, DiMauro S, De Vivo DC. Varying loads of the mitochondrial DNA A3243G mutation in different tissues: implications for diagnosis. *Am J Med Genet A* 2004;**130**:134–7.
28. **Whittaker RG,** Blackwood JK, Alston CL, Blakely EL, Elson JL, McFarland R, Chinnery PF, Turnbull DM, Taylor RW. Urine heteroplasmy is the best predictor of clinical outcome in the m.3243A>G mtDNA mutation. *Neurology* 2009;**72**:568–9.
29. **Ohno K,** Yamamoto M, Engel AG, Harper CM, Roberts LR, Tan GH, Fatourechi V. MELAS and Kerns-Sayre-type communication with myopathy and autoimmune polyendocrinopathy. *Ann Neurol* 1996;**39**:761–6.

Epilepsy Research (2010) 90, 199–206

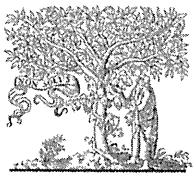

journal homepage: www.elsevier.com/locate/epilepsyres

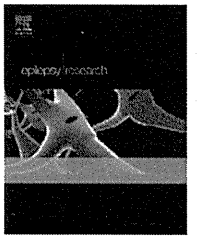

The applications of time-frequency analyses to ictal magnetoencephalography in neocortical epilepsy

Kazuyori Yagyu[a,*], Fumiya Takeuchi[b], Hideaki Shiraishi[a], Shingo Nakane[c], Keitaro Sueda[a], Naoko Asahina[a], Shinobu Kohsaka[a], Shuichi Umeoka[d], Naotaka Usui[d], Koichi Baba[d], Shinji Saitoh[a]

[a] *Department of Pediatrics, Hokkaido University Graduate School of Medicine, Japan*
[b] *Faculty of Health Sciences, Hokkaido University Graduate School of Health Sciences, Japan*
[c] *Division of Magnetoencephalography, Hokkaido University Hospital, Japan*
[d] *Department of Neurosurgery, National Epilepsy Center, Shizuoka Institute of Epilepsy and Neurological Disorders, Japan*

Received 14 June 2009; received in revised form 13 January 2010; accepted 2 May 2010
Available online 1 June 2010

KEYWORDS
Ictal onset;
Propagation;
Polyspike;
Short-time Fourier transform;
Ictal discharge;
Rhythmic activities

Summary
Purpose: Ictal magenetoencephalographic (MEG) discharges convey significant information about ictal onset and propagation, but there is no established method for analyzing ictal MEG. This study sought to clarify the usefulness of time-frequency analyses using short-time Fourier transform (STFT) for ictal onset and propagation of ictal MEG activity in patients with neocortical epilepsy.
Methods: Four ictal MEG discharges in two patients with perirolandic epilepsy and one with frontal lobe epilepsy (FLE) were evaluated by time-frequency analyses using STFT. Prominent oscillation bands were collected manually and the magnitudes of those specific bands were superimposed on individual 3D-magnetic resonance images.
Results: STFT showed specific rhythmic activities from alpha to beta bands at the magnetological onset in all four ictal MEG records. Those activities were located at the vicinity of interictal spike sources, as estimated by the single dipole method (SDM), and two of the four ictal rhythmic activities promptly propagated to ipsilateral or bilateral cerebral cortices. The patients with FLE and perirolandic epilepsy underwent frontal lobectomy and resection of primary motor area, respectively including the origin of high-magnitude areas of a specific band indicated by STFT, and have been seizure free after the surgery.

* Corresponding author at: Department of Pediatrics, Hokkaido University Graduate School of Medicine, North 15, West 7, Kita-ku, Sapporo, Hokkaido 060-8638, Japan. Tel.: +81 11 706 5954; fax: +81 11 706 7898.
E-mail address: kazuyori@med.hokudai.ac.jp (K. Yagyu).

0920-1211/$ – see front matter
doi:10.1016/j.eplepsyres.2010.05.001

Conclusions: STFT for ictal MEG discharges readily demonstrated the ictal onset and propagation. These data were important for decisions on surgical procedure and extent of resection. Ictal MEG analyses using STFT could provide a powerful tool for noninvasive evaluation of ictal onset zone.

Introduction

Precise localization of ictal onset and propagation in patients with symptomatic localization-related epilepsy (SLRE) is critical, especially in candidates for epilepsy surgery. Magnetoencephalography (MEG) is a new tool for assessing epileptic current that shows superior spatial and temporal resolution over the standard EEG (Hämäläinen et al., 1993). The single dipole method (SDM) is a useful way to monitor interictal MEG epileptiform activity (Stefan et al., 2003), although a method for analyzing MEG-measured ictal activity has not been established.

The ictal onset area was successfully demonstrated in cases with epilepsia partialis continua using a combination of jerk-locked back averaging and SDM with MEG (Shigeto et al., 1997; Oishi et al., 2002a). Tilz et al. (2002) also analyzed ictal MEG activities by SDM for epileptic patients that predominantly experienced mesial temporal lobe epilepsy. This study determined the ictal onset area successfully in 6 out of 13 cases, while SDM was not available in the remaining patients. In another study of MEG analyses for ictal rhythmic activities in four cases with medial frontal lobe epilepsy (FLE), SDM was not applicable for two of these cases, while one case had no significant spike at the onset zone in ictal MEG discharges, and the remaining patient showed no reliable spike sources by SDM (Shiraishi et al., 2001). The latter two cases were considered inapplicable for the SDM formula because the signals had already propagated broadly. Jongh et al. (2003) concluded that in patients with SLRE and brain tumor, interictal fast activities of 8–50 Hz did not localize to the tumor borders, and that SDM was not useful for analyzing fast waves in such cases.

SDM is an established procedure for analyzing single or spatially and temporally limited activities such as interictal epileptiform activities; however, it has limitations for analyzing spatially propagated and temporally prolonged rhythmic magnetological activity including ictal data during the secondary generalization. Nevertheless, ictal activities contain valuable information (Tilz et al., 2002; Jongh et al., 2003), and a reliable confirmatory method for analyzing ictal MEG is needed.

Rhythmic ictal discharge of EEG in SLRE reflects the precise location of ictal onset (Westmoreland, 1998; Verma and Radtke, 2006). Furthermore, Guggisberg et al. (2008) recently reported that fast oscillations associated with interictal spikes in MEG detected by spike-locked frequency analysis successfully demonstrated the localized epileptogenic zone.

The present study analyzed the localization of ictal rhythmic activity onset and propagation using time-frequency analysis by short-time Fourier transform (STFT) in patients with neocortical epilepsy. The locations of specific-frequency bands were also correlated with conventional SDM results for interictal epileptiform spikes sources and with prognosis following surgical treatment.

Patients and methods

Patients

Case 1. A 12-year-old girl with FLE. She had a past history of neonatal left-middle cerebral artery infarction. Seizures started at the age of 3 years presented as atonic seizure on the right side of her body, and postural seizure with right-limb extension. Her seizures occurred daily even with multiple antiepileptic drugs (AEDs). Brain MRI revealed an encephalomalacia at the left-frontal and parietal lobes (Fig. 1A, left).

Case 2. A 14-year-old boy with perirolandic epilepsy. His seizures started at the age of 8 years, beginning with somatosensory auras (tingling in the right hand) and evolving into right hemiconvulsion with his face and eyes deviated to the right side. His seizures were precipitated by touch on the right side of his body and occurred daily even with multiple AEDs. Brain MRI demonstrated no abnormality. [18F]-fluorodeoxyglucose positron emission tomography (FDG-PET) showed glucose hypometabolism at the left postcentral gyrus (Fig. 2A).

Case 3. A 25-year-old woman with perirolandic epilepsy. Her seizures started at the age of 10 years, beginning with somatosensory auras in the left ear and evolving into complex partial seizures. The seizures were always precipitated by touch on the left side of her body and occurred daily in spite of multiple AEDs. She had no brain lesion on MRI or [18F]-FDG-PET.

In all cases, guardians gave written informed consent for this study.

MEG data analyses

MEG data were recorded using a 204-channel, helmet-shaped gradiometer (Vectorview System, Elekta-Neuromag Oy, Stockholm, Sweden) from patients in a supine position in a magnetically shielded room, and collected for about 40 min from each patient using a 600-Hz sampling rate. During the MEG recording, scalp EEGs were also recorded simultaneously using the international 10–20 system.

The segments containing ictal and interictal paroxysms were selected manually. The raw MEG data were filtered with band-pass filtering of 0.03–133 Hz for offline analyses. We used SDM for localized interictal epileptiform activities and STFT for ictal rhythmic polyspike epileptiform discharges to determine the onset and propagation of the ictal discharges.

Single dipole method (SDM)

Dipole-fit software (Neuromag Oy, Helsinki, Finland) was used to calculate the equivalent current dipoles (ECDs). We defined acceptable ECDs by a goodness of fit (GOF) higher than 70%; this value measures how well the ECD model explains the measured signals. Acceptable ECDs were superimposed on the individual MRIs.

Short-time Fourier transform (STFT) analyses

STFT was used to show the distribution of MEG polyspikes (Oppenheim and Schafer, 1999) and the MATLAB (MathWorks, Natick, MA, USA) program was used to apply STFT to the MEG signals. Each signal was divided into defined sequential frames, and fast Fourier transformation (FFT) was applied to each frame.

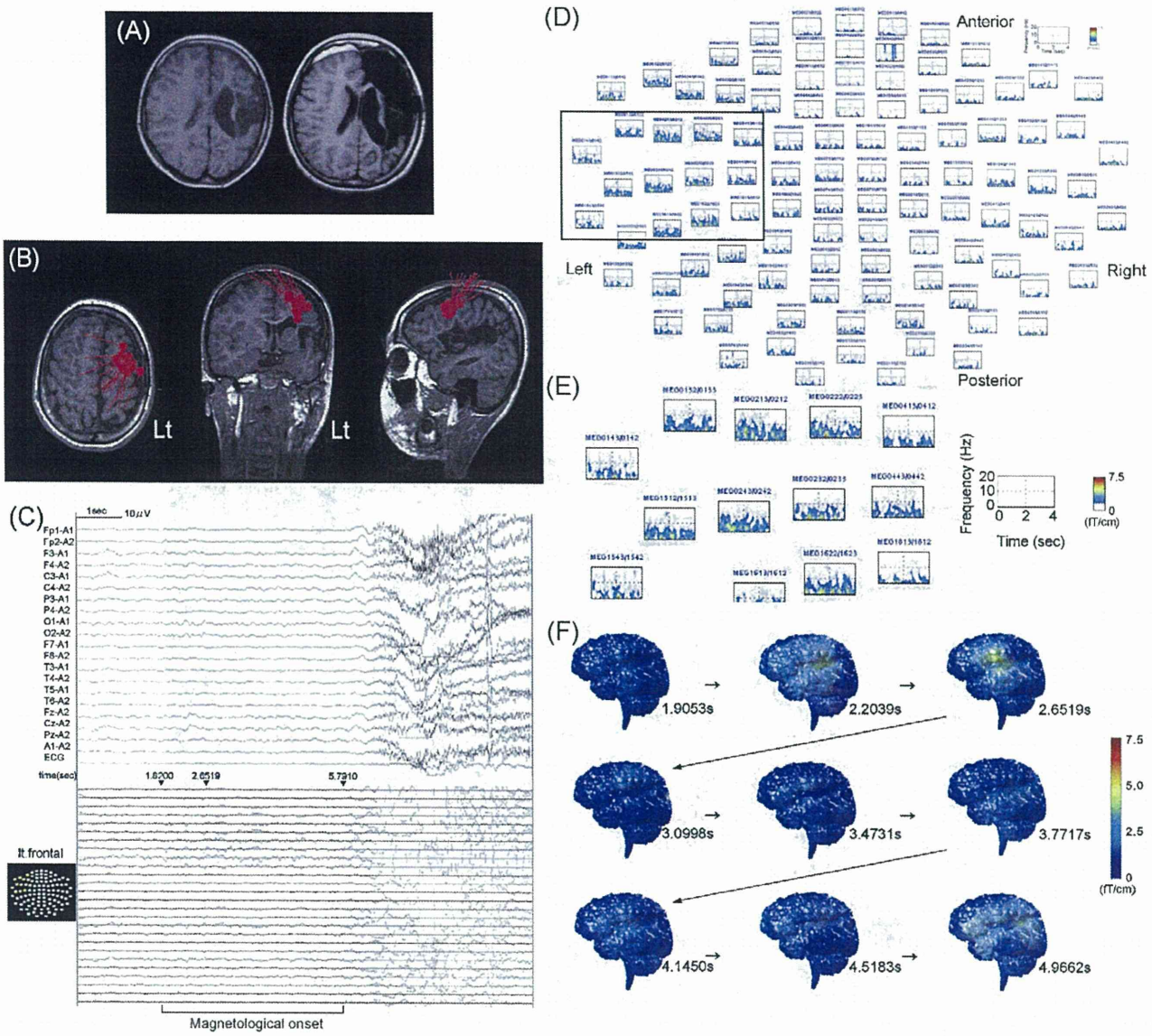

Figure 1 (A) Case 1 MRI: MRI before (left) and after (right) the operation showed encephalomalacia in the left hemisphere (left) and an operation scar in the left-frontal lobe (right). (B) Case 1 SDM: Interictal spike sources were estimated to lie near the posterior lateral area of the left-frontal lobe (red dot). (C) Case 1 ictal EEG and MEG: representative ictal EEG (top) showing a left-frontal slow wave followed by left-frontal dominant polyspikes; MEG at the left-frontal area (bottom) showing rhythmic discharges with a 7–20-Hz band oscillation (magnetological onset). (D) Case 1 MEG/STFT: analysis of graph by STFT for magnetological onset duration of (C) (4.0 s), showing up to 12-Hz oscillations at the left-frontal area. (E) Case 1 MEG/STFT: representative STFT illustration of MEG channel at the left-frontal area (corresponding to the boxed area of (D)) showing specific oscillations of up to 12 Hz (yellow and red areas). (F) Case 1 3D-MRI overlay: sequential demonstration of specific-frequency band magnitudes projected on 3D-MRIs. Color bar indicates the magnitude of a specific-frequency band and numbers on the right lower part demonstrate the time scale corresponding to (C). (For interpretation of the references to color in this figure legend, the reader is referred to the web version of the article.)

In the present study, STFT was implemented using a 256-point window. The time of each window was 426.7 ms (i.e., 256 points × 1000 ms/600 Hz), and the window was shifted every four points, which corresponded to 6.7 ms (i.e., 1000 ms/600 Hz × 4 points). FFT applied to each window. This process was repeated for all selected signals. The time-frequency distributions are displayed graphically.

Selection of specific-frequency bands and projection to 3D-MRIs

The time-frequency distributions were analyzed up to 133 Hz and for 10 s until ictal motion artifact started. Specific-frequency bands that appeared continuously and were prominent from background activities were selected man-

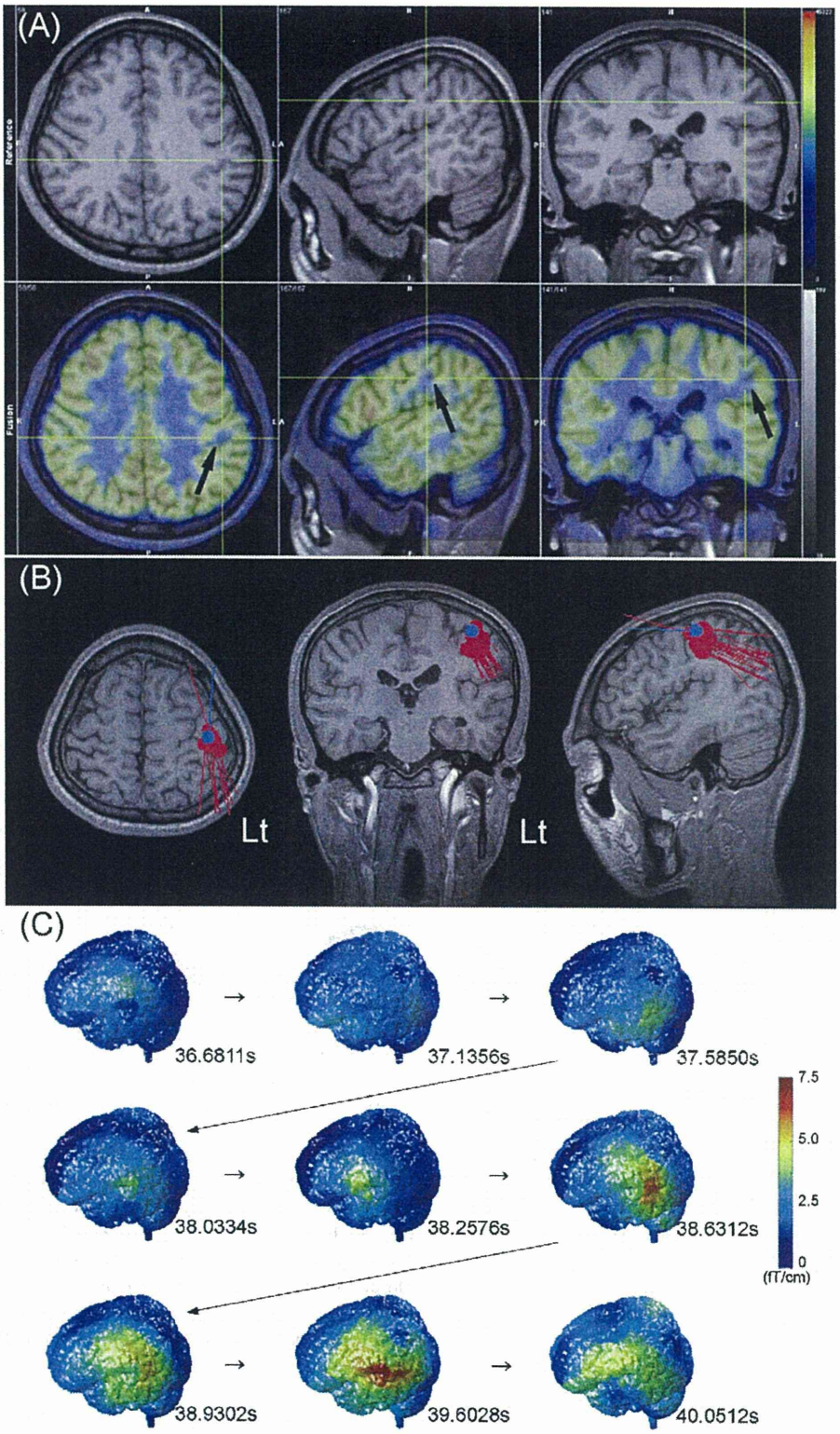

Figure 2 (A) Case 2 [18F]-FDG-PET: MRI (top) and [18F]-FDG-PET (bottom) showing hypometabolism of glucose consumption at the left postcentral gyrus (arrow). (B) Case 2 SDM: blue dot indicates somatosensory-evoked field and red dots indicate spike sources estimated by SDM. Those spike sources were estimated in the left postcentral gyrus. (C) Case 2 3D-MRI overlay: high-magnitude zone of 10—15 Hz oscillation was generated from the left parietal and temporal lobes and followed by propagation to the bilateral temporal and parietal lobes. Color mapping of 3D-MRI indicates the magnitudes of specific-frequency bands (10—15 Hz). (For interpretation of the references to color in this figure legend, the reader is referred to the web version of the article.)

ually. Thus, the duration of graphs and selected bands varied.

The specific-frequency bands selected were then projected to individual 3D-MRIs. The power spectrum of these bands on 3D-MRI was located at the intersection of the line beneath the planer gradiometer coil and brain surface.

Electrocorticography (ECoG)

To define the epileptogenic focus, chronic subdural electrodes were implanted to analyze the location of ictogenesis, according to the interictal and ictal scalp EEG and MEG results. Electrocorticography (ECoG) was conducted using Neurofax-1000 (Nihon-Kohden, Tokyo, Japan) amplifiers at a sampling rate of 1 kHz and time constant at 10 s with grid platinum/iridium electrodes (2.3-mm diameter, 10-mm inter-electrode spacing, Ad-Tech, Racine, WI). High frequent oscillation (HFO) was analyzed by ECoG, with 53–300 Hz band-pass filtering.

Results

Case 1

The interictal EEG showed left-frontal dominant polyspikes, polyspikes and wave complex. SDM analysis of the MEG showed clustered spike sources at the left-frontal lobe in the vicinity of the encephalomalacia (Fig. 1B). Ictal EEG showed left-frontal slow waves followed by left-frontal dominant polyspikes (Fig. 1C, top).

Ictal MEG data with 4.0 s prior to ictal motion artifact analyzed by STFT (Fig. 1C, bottom) showed left-frontal dominant rhythmic magnetological activities of 7–12 Hz (Fig. 1D and E). These high-magnitude areas of activity were located at the left superior-frontal gyrus on 3D-MRI (Fig. 1F), which was consistent with the spike sources estimated by SDM (Fig. 1B). We also applied SDM to the ictal MEG data; however, ECDs were scattered broadly over the left-frontal to occipital lobe regions and GOF was generally very low (<50%). Based on the STFT results and other noninvasive examinations, we predicted the ictal onset zone location as anterior to the ischemic scar.

After noninvasive presurgical evaluation, the patient underwent long-term intracranial EEG monitoring with subdural electrodes. Electrical stimulation in the vicinity of the left premotor area induced the patient's habitual seizure. The ictal ECoG were captured once and a low-amplitude HFO of 200–300 Hz was detected at the superior-frontal gyrus in pre-ictal period. She underwent frontal lobectomy including the high-magnitude areas of the ictal MEG (Fig. 1A, right). She has been seizure free for a year since surgery and has no mental or motor deficit.

Case 2

This patient showed left central and parietal spikes interictally by EEG. SDM analysis of the interictal MEG showed clustered spike sources at the left postcentral gyrus (Fig. 2B).

Ictal EEG demonstrated diffuse 10-Hz polyspikes bilaterally. Analysis of the ictal MEG data with 4.0 s duration prior to ictal motion artifact by STFT showed specific rhythmic activities of 10–15 Hz at the magnetological onset of the seizure. Those ictal activities originated from the left parietal and temporal lobes, and propagated to the bilateral parietal and temporal lobes (Fig. 2C). The ictal onset zone defined by ictal MEG was in the vicinity of interictal spike sources estimated by SDM. This result was consistent also with the localization of glucose hypometabolism indicated by [18F]-FDG-PET (Fig. 2A). The SDM of this patient's ictal MEG located ECDs at the perirolandic area and deep white matter at the bilateral temporal and parietal lobes.

This patient underwent long-term intracranial EEG monitoring with subdural electrodes at the age of 15. Interictally, spikes were seen over the precentral and postcentral gyri, and ictal ECoG also revealed ictal onset zone at the precentral and postcentral gyri, corresponding to the ictal high-magnitude area of rhythmic activity assessed by STFT and spike sources estimated by SDM. His ictal ECoG was captured 10 times, showing a HFO of >200 Hz intermittently at the supplementary motor area in the pre-ictal period that disappeared in the ictal period. The ECoG also detected the earliest activity in the primary motor area. We therefore proposed that the ictogenesis was located near the primary motor area, although ictal activity indicated bilateral propagation on MEG. Since the ictogenesis was supposed to be in the eloquent area in this case, the patient underwent only partial resection at the primary motor area. His seizures gradually decreased and disappeared completely within 1 year.

Case 3

Interictal EEG showed right central and parietal spikes. Interictal MEG showed clustered spike sources at the right postcentral gyrus by SDM (Fig. 3A). In the first seizure, the ictal EEG demonstrated bilateral frontal and central dominant 12–15-Hz polyspikes. In the second seizure, the ictal EEG showed right-frontal and temporal dominant 15-Hz polyspikes.

Ictal rhythmic activities were obtained from the first seizure of 4.0 s duration and the second one lasting 2.9 s, prior to the accumulation of ictal motion artifact. STFT showed specific rhythmic activities of 10–20 Hz at magnetological onset in the first seizure and 10–15 Hz in the second seizure. Rhythmic activities in the first seizure were generated from the right parietal and temporal lobes; they promptly propagated to the bilateral parietal and temporal lobes (Fig. 3B). Analysis of the same ictal data by SDM located ECDs in the deep white matter of the right parietal and occipital lobes, indicating no bilateral propagation. In the second seizure, rhythmic activity was also generated from right parietal and temporal lobes, however, propagation was limited to the ipsilateral parietal and temporal lobes (Fig. 3C). Analyzed by SDM located these ECDs in the deep white matter of the right parietal and temporal lobes. Both in two ictal MEG, rhythmic activities originated in the vicinity of the interictal spike sources as estimated by SDM.

Discussion

Frequency analyses to ictal MEG

This study indicated that frequency analyses using STFT to ictal MEG provide information about ictogenesis (cases

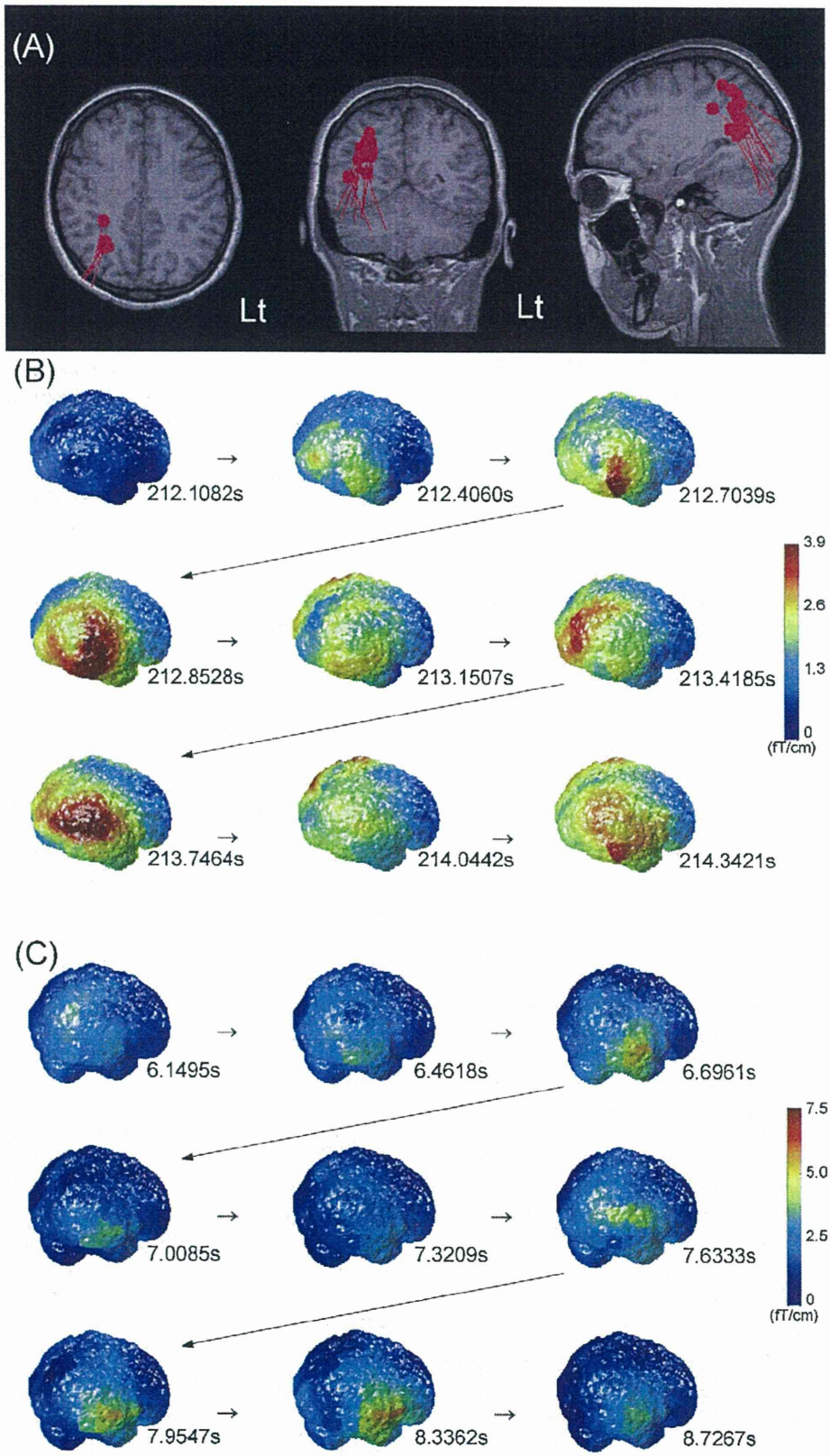

Figure 3 (A) Case 3 SDM: spike sources are clustered at the right postcentral gyrus. (B) Case 3 first seizure 3D-MRI overlay: high-magnitude zone of 10–20 Hz oscillation projected to 3D-MRI. High-magnitude area starts at the right parietal and temporal lobes and promptly propagates to the bilateral temporal and parietal lobes. (C) Case 3 second seizure 3D-MRI overlay: high-magnitude zone of 10–15 Hz oscillation generated from the right parietal and temporal lobes; these propagations were limited.

1 and 2) and visualize dynamic changes in ictal activities (cases 2 and 3). Our method thus has practical applications for analyzing ictal rhythmic magnetological activity. Another advantage of the method was the lack of issue with the inverse problem, as different from SDM, meaning that rhythmic epileptiform activities could be evaluated directly without presupposition.

Limitations of SDM

Our study revealed two problems with SDM for analyzing ictal MEG. First, the ECDs had only low GOF value, with spike sources not generated from a localized area or the subjective spike having low signal to noise ratio. Second, most of the ECDs were estimated in the deep white matter, resulting in abnormal current being generated from a wide area simultaneously.

The localization of an ECD can be calculated only when a 3 cm^2 or wider area of cerebral cortex is synchronously activated (Oishi et al., 2002b). The site of ECD could also be misleading if too wide an area is simultaneously activated, as in this study. Therefore, the activated areas of the cortex should be limited to obtain an acceptable ECD. SDM uses an inverse problem formula based on the hypothesis that the spike is generated from a localized area; it is therefore not applicable for multiple spikes generated simultaneously or spikes originating from deep or very broad areas. Time-frequency analysis has the advantage of not needing to solve the inverse problem.

Rhythmic activities in MEG

Rhythmic activities indicate ictal onset zones on scalp EEG and electrocorticography (ECoG). However, scalp EEG has limited value in showing the precise location of ictal onset because the voltage declines via the cerebrospinal fluid and cranium. ECoG remains the gold standard for defining the location of seizure origin (Worrell et al., 2004), but it cannot be used for routine evaluation. In patients with focal cortical dysplasia, rhythmic epileptic discharges on EEG accorded well with the continuous epileptic discharges on ECoG (Gambardella et al., 1996). Dalal et al. (2008) also reported good coherence of both beta band (12—30 Hz) and high gamma band (65—90 Hz) between MEG and ECoG by self-paced finger-movement tasks. Their work indicated that MEG is equivalent to ECoG for evaluating epileptic rhythmic activities. The present study indicated that MEG analysis using STFT could provide valuable information on ictal onset zones. Using this method, the rhythmic activities successfully localized the origin of ictus and were colocalized with interictal discharges estimated by SDM. This finding emphasized the clinical value of routine interictal MEG analysis. In two patients (cases 1 and 2), the localization of rhythmic activities was concordant with the ECoG findings and surgical resection including the high-magnitude areas of the ictal MEG rendered the patient seizure free. This result may suggest the usefulness of STFT for deciding the area of surgical resection.

Visualization of ictal activity

Ictal STFT in two instances reported here (case 2 and the first seizure of case 3) showed that ictal rhythmic activities propagated promptly to contralateral homotopic areas, then went to and fro between the hemispheres, before finally spreading out broadly throughout the brain. In other words, the propagation of ictal activities was well visualized by STFT analyses. Although ECoG analysis is regarded as the gold standard for precise evaluation of epileptic current, MEG analysis has an advantage over ECoG in analyzing changes in epileptic discharges over the entire cerebral cortices, noninvasively and repeatedly. Götz-Trabert et al. (2008) successfully evaluated the propagation of ictal activity in patients with mesial temporal lobe epilepsy and neocortical epilepsy using ECoG with success in depicting the propagation of ictal activity. However, these authors also reported that intracranial EEG monitoring was limited in cerebral capacity and in investigating the invasion of contralateral hemispheres. The current results thus indicated another clinical value of MEG for ictal study.

High-frequency oscillation (HFO)

In cases 1 and 2, although ictal ECoG showed over 200-Hz HFO, it was not feasible to detect over 30 Hz by SFT analyses of MEG in this study.

HFO were recently detected on ictal ECoG by Jirsch et al. (2006), with very good coincidence of a localized area of high-frequency band (250—500 Hz) in the ECoG and ictal onset zone. This was an obvious limitation of MEG compared with ECoG, because spontaneous MEG recordings require synchronous activity among large assemblies of neurons and is therefore not able to detect very fine neurological activity (Pfurtscheller and Silva, 1999). However, improvements in distance between sensor and ictal activity onset zone or sensor density might reduce this limitation of MEG.

Conclusion

In conclusion, STFT is a new method for analyzing onset and propagation of ictal activities in whole brain. MEG is potentially as valuable as ECoG, and ictal MEG analyses using STFT could become a powerful tool for noninvasive evaluation of ictal onset zones, especially in candidates for surgical treatment of epilepsy.

Conflict of interest

The authors have no conflicts of interest.

Acknowledgement

We thank Prof. Tadashi Ariga of the Department of Pediatrics, Hokkaido University Graduate School of Medicine, for his valuable editorial opinion.

References

Dalal, S.S., Guggisberg, A.G., Edwards, E., Sekihara, K., Findlay, A.M., Canotly, R.T., Berger, M.S., Knight, R.T., Barbaro, N.M., Kirsch, H.E., Nagarajan, S.S., 2008. Five-dimensional neuroimaging: localization of the time-frequency dynamics of cortical activity. Neuroimage 40, 1686–1700.

Gambardella, A., Palmini, A., Andermann, F., Dubeau, F., Costa, J.C.D., Quesney, L.F., Andermann, E., Olivier, A., 1996. Usefulness of focal rhythmic discharges on scalp EEG of patients with focal cortical dysplasia and intractable epilepsy. Electroencephalogr. Clin. Neurophysiol. 98, 243–249.

Götz-Trabert, K., Hauck, C., Wagner, K., Fauser, S., Schlze-Bonhage, A., 2008. Spread of ictal activity in focal epilepsy. Epilepsia 49, 1594–1601.

Guggisberg, A.G., Kirsch, H.E., Mantle, M.M., Barbaro, N.M., Nagarajan, S.S., 2008. Fast oscillation associated with interictal spikes localize the epileptogenic zone in patients with partial epilepsy. Neuroimage 30, 661–668.

Hämäläinen, M.S., Hari, R., Ilmoniemi, R.J., Knuutila, J., Lounasmaa, O.V., 1993. Magnetoencephalography – theory, instrumentation, and applications to noninvasive studies of the working brain. Rev. Mod. Phys. 65, 413–497.

Jirsch, J.D., Urrestarazu, E., LeVan, P., Olivier, A., Dubeau, F., Gotman, J., 2006. High-frequency oscillations during human focal seizures. Brain 129, 1593–1608.

Jongh, A.D., Munck, J.C.D., Baayen, J.C., Puligheddu, M., Jonkman, E.J., Stam, C.J., 2003. Localization of fast MEG waves in patients with brain tumors and epilepsy. Brain Topogr. 15, 173–179.

Oishi, A., Tobimatsu, S., Ochi, H., Ohyagi, Y., Kubota, T., Taniwaki, T., Yamamoto, T., Furuya, H., Kira, J., 2002a. Paradoxical lateralization of parasagittal spikes revealed by back averaging of EEG and MEG in a case with epilepsia partialis continua. J. Neurol. Sci. 193, 151–155.

Oishi, M., Otsubo, H., Kameyama, S., Morota, N., Masuda, H., Kitayama, M., Tanaka, R., 2002b. Epileptic spikes: magnetoencephalography versus simultaneous electrocorticography. Epilepsia 43, 1390–1395.

Oppenheim, A., Schafer, R.W., 1999. Discrete-Time Signal Processing. Prentice Hall, New Jersey.

Pfurtscheller, G., Silva, F.H.L., 1999. Event-related EEG/MEG synchronization and desynchronization: basic principles. Clin. Neurophysiol. 110, 1842–1857.

Shigeto, H., Tobimatsu, S., Morioka, T., Yamamoto, T., Kobayashi, T., Kato, M., 1997. Jerk-locked back averaging and dipole source localization of magnetoencephalographic transients in a patient with epilepsia partialis continua. Electroencephalogr. Clin. Neurophysiol. 103, 440–444.

Shiraishi, H., Watanabe, Y., Watanabe, M., Inoue, Y., Fujiwara, T., Yagi, K., 2001. Interictal and ictal magnetoencephalographic study in patients with medial frontal lobe epilepsy. Epilepsia 42, 875–882.

Stefan, H., Hummel, C., Scheler, G., Genow, A., Druschky, K., Tilz, C., Kaltenhäuser, M., Hopfengärtner, R., Buchfelder, M., Romstöck, J., 2003. Magnetic brain source imaging of focal epileptic activity: a synopsis of 455 cases. Brain 126, 2396–2405.

Tilz, C., Hummel, C., Kettenmann, B., Stefen, H., 2002. Ictal onset localization of epileptic of epileptic seizures by magnetoencephalography. Acta Neurol. Scand. 106, 190–195.

Verma, A., Radtke, R., 2006. EEG of partial seizures. J. Clin. Neurophysiol. 23, 333–339.

Westmoreland, B.F., 1998. The EEG finding in extratemporal seizures. Epilepsia 39 (Suppl. 4), S1–S8.

Worrell, G.A., Parish, L., Cranstoun, S.D., Jonas, R., Baltuch, G., Litt, B., 2004. High-frequency oscillations and seizure generation in neocortical epilepsy. Brain 127, 1496–1506.

Short report

Parthenogenetic chimaerism/mosaicism with a Silver-Russell syndrome-like phenotype

K Yamazawa,[1,2] K Nakabayashi,[3] M Kagami,[1] T Sato,[1] S Saitoh,[4] R Horikawa,[5] N Hizuka,[6] T Ogata[1]

► Additional figures, tables and an appendix are published online only. To view these files, please visit the journal online (http://jmg.bmj.com).

[1]Departments of Endocrinology and Metabolism, National Research Institute for Child Health and Development, Tokyo, Japan
[2]Department of Physiology, Development & Neuroscience, University of Cambridge, Cambridge, UK
[3]Maternal-Fetal Biology, National Research Institute for Child Health and Development, Tokyo, Japan
[4]Department of Pediatrics, Hokkaido University Graduate School of Medicine, Sapporo, Japan
[5]Division of Endocrinology and Metabolism, National Children's Hospital, Tokyo, Japan
[6]Department of Medicine, Institute of Clinical Endocrinology, Tokyo Women's Medical University, Tokyo, Japan

Correspondence to
Dr Tsutomu Ogata, Department of Endocrinology and Metabolism, National Research Institute for Child Health and Development, 2-10-1 Ohkura, Setagaya, Tokyo 157-8535, Japan; tomogata@nch.go.jp

Received 20 March 2010
Revised 6 May 2010
Accepted 8 May 2010
Published Online First
3 August 2010

ABSTRACT

Introduction We report a 34-year-old Japanese female with a Silver-Russell syndrome (SRS)-like phenotype and a mosaic Turner syndrome karyotype (45,X/46,XX).

Methods/Results Molecular studies including methylation analysis of 17 differentially methylated regions (DMRs) on the autosomes and the *XIST*-DMR on the X chromosome and genome-wide microsatellite analysis for 96 autosomal loci and 30 X chromosomal loci revealed that the 46,XX cell lineage was accompanied by maternal uniparental isodisomy for all chromosomes (upid(AC)mat), whereas the 45,X cell lineage was associated with biparentally derived autosomes and a maternally derived X chromosome. The frequency of the 46,XX upid(AC)mat cells was calculated as 84% in leukocytes, 56% in salivary cells, and 18% in buccal epithelial cells.

Discussion The results imply that a parthenogenetic activation took place around the time of fertilisation of a sperm missing a sex chromosome, resulting in the generation of the upid(AC)mat 46,XX cell lineage by endoreplication of one blastomere containing a female pronucleus and the 45,X cell lineage by union of male and female pronuclei. It is likely that the extent of overall (epi)genetic aberrations exceeded the threshold level for the development of SRS phenotype, but not for the occurrence of other imprinting disorders or recessive Mendelian disorders.

Although a mammal with maternal uniparental disomy for all chromosomes (upd(AC)mat) is incompatible with life because of genomic imprinting,[1] a mammal with a upd(AC)mat cell lineage could be viable in the presence of a co-existing normal cell lineage. In the human, Strain *et al*[2] have reported 46,XX peripheral blood cells with maternal uniparental isodisomy for all chromosomes (upid(AC)mat) in a 1.2-year-old phenotypically male patient with aggressive behaviour, hemifacial hypoplasia and normal birth weight. Because of the 46,XX disorders of sex development, detailed molecular studies were performed, revealing the presence of a normal 46,XY cell lineage in a vast majority of skin fibroblasts and a upid(AC)mat 46,XX cell lineage in nearly all blood cells. In addition, although the data are insufficient to draw a definitive conclusion, Horike *et al*[3] have also identified 46,XX peripheral blood cells with possible upd(AC)mat in a phenotypically male patient through methylation analyses for plural differentially methylated regions (DMRs) in 11 patients with Silver–Russell syndrome (SRS)-like phenotype. This patient was found to have a normal 46,XY cell lineage and a triploid 69,XXY cell lineage in skin fibroblasts.

However, such patients with a upd(AC)mat cell lineage remain extremely rare, and there is no report describing a human with such a cell lineage in the absence of a normal cell lineage. Here, we report a female patient with a upid(AC)mat 46,XX cell lineage and a non-upd 45,X cell lineage who was identified through genetic screenings of 103 patients with SRS-like phenotype.

MATERIALS AND METHODS

Case report

This Japanese female patient was conceived naturally and born at 40 weeks of gestation by a normal vaginal delivery. At birth, her length was 44.0 cm (−3.1 SD), her weight 2.1 kg (−2.9 SD) and her occipitofrontal head circumference (OFC) 30.5 cm (−2.3 SD). The parents and the younger brother were clinically normal (the father died from a traffic accident).

At 2 years of age, she was referred to us because of growth failure. Her height was 77.7 cm (−2.5 SD), her weight 8.45 kg (−2.6 SD) and her OFC 43.5 cm (−2.5 SD). Physical examination revealed several SRS-like somatic features such as triangular face, right hemihypoplasia and bilateral fifth finger clinodactyly. She also had developmental retardation, with a developmental quotient of 56. Endocrine studies for short stature were normal as were radiological studies. Cytogenetic analysis using lymphocytes indicated a low-grade mosaic Turner syndrome (TS) karyotype, 45,X[3]/46,XX[47]. Thus, a screening of TS phenotype[4] was performed, detecting horseshoe kidney but no body surface features or cardiovascular lesion. Chromosome analysis was repeated at 6 and 32 years of age using lymphocytes, revealing a 45,X[8]/46,XX[92] karyotype and a 45,X[12]/46,XX[88] karyotype, respectively. On the last examination at 34 years of age, her height was 125.0 cm (−6.2 SD), her weight 37.5 kg (−2.0 SD) and her OFC 51.2 cm (−2.8 SD). She was engaged in a simple work and was able to get on her daily life for herself.

Sample preparation

This study was approved by the Institutional Review Board Committees at National Center for Child health and Development. After obtaining written informed consent, genomic DNA was extracted from leukocytes of the patient, the mother and the brother and from salivary cells, which comprise ~40% of buccal epithelial cells and ~60% of leukocytes,[5] of the patient. Lymphocyte metaphase spreads and leukocyte RNA were also

obtained from the patient. Leukocytes of healthy adults and patients with imprinting disorders were utilised for controls.

Primers and probes

The primers utilised in this study are summarised in supplementary methods and supplementary tables 1–3.

DMR analyses

We first performed bio-combined bisulfite restriction analysis (COBRA)[6] and bisulfite sequencing of the *H19*-DMR (A) on chromosome 11p15.5 by the previously described methods[7] and methylation-sensitive PCR analysis of the *MEST*-DMR (A) on chromosome 7q32.2 by the previously described methods[8] with minor modifications (the methylated and unmethylated allele-specific primers were designed to yield PCR products of different sizes, and the PCR products were visualised on the 2100 Bioanalyzer (Agilent, Santa Clara, California, USA)). This was because hypomethylation (epimutation) of the normally methylated *H19*-DMR of paternal origin and maternal uniparental disomy 7 are known to account for 35–65% and 5–10% of SRS patients, respectively.[9 10] In addition, fluorescence in situ hybridisation (FISH) analysis was performed with a ~84-kb RP5-998N23 probe containing the *H19*-DMR (BACPAC Resources Center, Oakland, California, USA). We also examined multiple other DMRs by bio-COBRA. The ratio of methylated clones (the methylation index) was calculated using peak heights of digested and undigested fragments on the 2100 Bioanalyzer using 2100 expert software.

Genome-wide microsatellite analysis

Microsatellite analysis was performed for 96 autosomal loci and 30 X chromosomal loci. The segment encompassing each locus was PCR-amplified, and the PCR product size was determined on the ABI PRISM 310 autosequencer using GeneScan software (Applied Biosystems, Foster City, California, USA).

PCR analysis for Y chromosomal loci

Standard PCR was performed for six Y chromosomal loci. The PCR products were electrophoresed using the 2100 Bioanalyzer.

Expression analysis

Quantitative real-time reverse transcriptase PCR analysis was performed for three paternally expressed genes (*IGF2*, *SNRPN* and *ZAC1*) and four maternally expressed genes (*H19*, *MEG3*, *PHLDA2* and *CDKN1C*) that are known to be variably (usually weakly) expressed in leukocytes (UniGene, http://www.ncbi.nlm.nih.gov/sites/entrez?db=unigene), using an ABI Prism 7000 Sequence Detection System (Applied Biosystems). *TBP* and *GAPDH* were utilised as internal controls.

RESULTS

DMR analyses

In leukocytes, the bio-COBRA indicated severely hypomethylated *H19*-DMR, and bisulfite sequencing combined with *rs2251375* SNP typing for 30 clones revealed maternal origin of 29 hypomethylated clones and non-maternal (paternal) origin of a single methylated clone in this patient (figure 1A). Thus, the marked hypomethylation of the *H19*-DMR was caused by predominance of maternally derived clones rather than hypomethylation of the *H19*-DMR of paternal origin. FISH analysis for 100 lymphocyte metaphase spreads excluded an apparent deletion of the paternally derived *H19*-DMR or duplication of the maternally derived *H19*-DMR (Supplementary figure 1). Methylation-sensitive PCR amplification for the *MEST*-DMR delineated a major peak for the methylated allele and a minor peak for the unmethylated allele (figure 1B). This also indicated the predominance of maternally derived clones and the co-existence of a minor portion of paternally derived clones. Furthermore, autosomal DMRs invariably exhibited markedly abnormal methylation patterns consistent with predominance of maternally inherited DMRs, whereas the methylation index of the *XIST*-DMR on the X chromosome remained within the female reference range (figure 1C). The abnormal methylation patterns were less obvious in salivary cells (thus, in buccal epithelial cells) than in leukocytes, except for the methylation index for the *XIST*-DMR that mildly exceeded the female reference range (figure 1A–C).

Microsatellite analysis

Major peaks consistent with maternal uniparental isodisomy and minor peaks of non-maternal (paternal) origin were identified for at least one locus on each autosome, with the minor peaks of non-maternal origin being more obvious in salivary cells than in leukocytes (figure 1D and supplementary table 4). Furthermore, the frequency of the upid(AC)mat cells was calculated as 84% in leukocytes, 56% in salivary cells and 18% in epithelial buccal cells, using the area under curves for the maternally and the non-maternally inherited peaks (supplementary note). Such minor peaks of non-maternal origin were not detected for all the 30 X chromosomal loci examined.

PCR analysis for Y chromosomal loci

PCR amplification failed to detect any trace of Y chromosome-specific bands in leukocytes and salivary cells (Supplementary figure 2).

Expression analysis

Expression analysis using control leukocytes indicated that, of the seven examined genes, *SNRPN* expression alone was strong enough to allow for a precise assessment (Supplementary figure 3). *SNRPN* expression was extremely low in this patient (figure 1E).

DISCUSSION

These results imply that this patient had a upid(AC)mat 46,XX cell lineage and a non-upd 45,X cell lineage. Indeed, methylation patterns of the *XIST*-DMR is explained by assuming that the two X chromosomes in the upid(AC)mat cells undergo random X-inactivation and that 45,X cells with the methylated *XIST*-DMR on a single active X chromosome[11] are relatively prevalent in buccal epithelial cells. Furthermore, lack of non-maternally derived minor peaks for microsatellite loci on the X chromosome is explained by assuming that the two X chromosomes in the upid(AC)mat cells and the single X chromosome in the 45,X cells are derived from a common X chromosome of maternal origin, with no paternally derived sex chromosome. It is likely, therefore, that a parthenogenetic activation took place around the time of fertilisation of a sperm missing a sex chromosome, resulting in the generation of the 46,XX cell lineage with upid (AC)mat by endoreplication (the replication of DNA without the subsequent completion of mitosis) of one blastomere containing a female pronucleus and the 45,X cell lineage with biparentally derived autosomes and a maternally derived X chromosome by union of male and female pronuclei (figure 2), although it is also possible that a paternally derived sex chromosome was present in the sperm but was lost from the normal

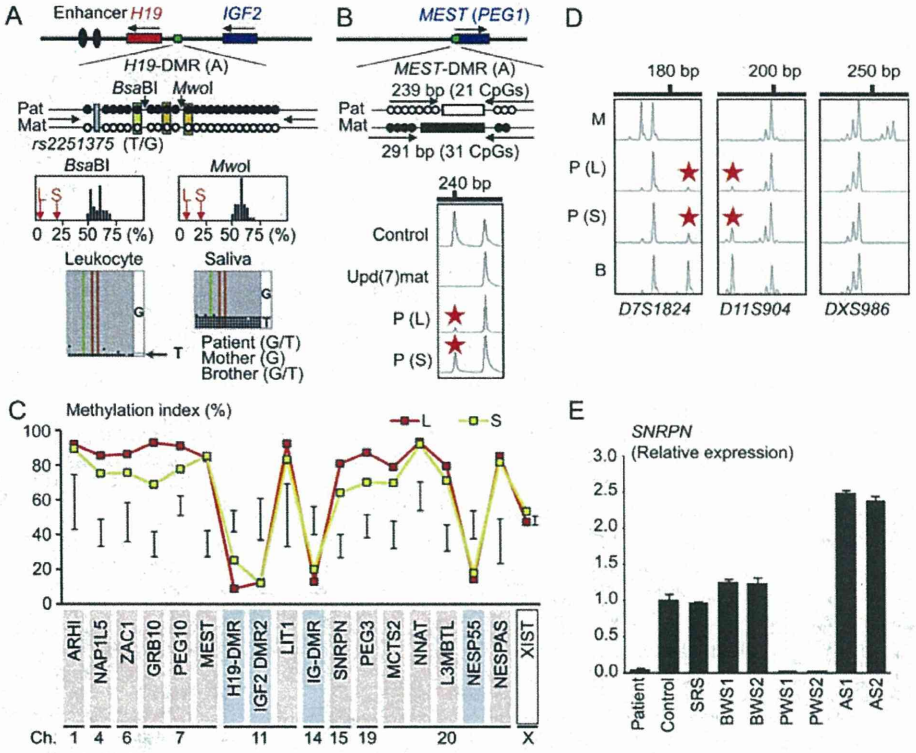

Figure 1 Representative molecular results. Pat, paternally derived allele; Mat, maternally derived allele; P, patient; M, mother; B, brother; L, leukocytes; and S, salivary cells. Filled and open circles in A and B represent methylated and unmethylated cytosine residues at the CpG dinucleotides, respectively. A. Methylation patterns of the *H19*-DMR (A) harbouring 23 CpG dinucleotides and the T/G SNP (*rs2251375*) (a grey box). The PCR products are digested with *Bsa*BI when the cytosine at the sixth CpG dinucleotide (highlighted in yellow) is methylated and with *Mwo*I when the two cytosines at the ninth and the 11th CpG dinucleotides (highlighted in orange) are methylated. For the bio-COBRA data, the black histograms represent the distribution of methylation indices (%) in 50 control participants, and L and S denote the methylation indices for leukocytes and salivary cells of this patient, respectively. For the bisulfite sequencing data, each line indicates a single clone. B. Methylated and unmethylated allele-specific PCR analysis for the *MEST*-DMR (A). In a control participant, the PCR products for methylated and unmethylated alleles are delineated, and the unequal amplification is consistent with a short product being more easily amplified than a long product. In a previously reported patient with upd(7)mat,[8] the methylated allele only is amplified. In this patient, major peaks for the methylated allele and minor peaks for the unmethylated allele (red asterisks) are detected. C. Methylation patterns for the 18 DMRs examined. The DMRs highlighted in blue and pink are methylated after paternal and maternal transmissions, respectively. The black vertical bars indicate the reference data (maximum–minimum) in 20 normal control participants, using leukocyte genomic DNA (for the *XIST*-DMR, 16 female data are shown). D. Representative microsatellite analysis. Minor peaks (red asterisks) have been identified for *D7S1824* and *D11S904* but not for *DXS986* of the patient. Since the peaks for *D7S1824* and *D11S904* are absent in the mother and clearly present in the brother, they are assessed to be of paternal origin. E. Relative expression level (mean ± SD) of *SNRPN* on chromosome 15. The data have been normalised against *TBP*. SRS, an SRS patient with an epimutation (hypomethylation) of the *H19*-DMR; BWS1, a BWS patient with an epimutation (hypermethylation) of the *H19*-DMR; BWS2, a BWS patient with upd(11)pat; PWS1, a PWS patient with upd(15)mat; PWS2, a PWS patient with an epimutation (hypermethylation) of the *SNRPN*-DMR; AS1, an Angelman syndrome (AS) patient with upd(15)pat; and AS2, an AS patient with an epimutation (hypomethylation) of the *SNRPN*-DMR.

cell lineage at the very early developmental stage. Hence, in a strict sense, this patient is neither a chimera resulting from the fusion of two different zygotes nor a mosaic caused by a mitotic error of a single zygote. In this regard, a triploid cell stage is assumed in the generation of a upid(AC)mat cell lineage, and such triploid cells may have been detected in skin fibroblasts of the patient reported by Horike *et al*.[3]

The upid(AC)mat cells accounted for the majority of leukocytes even in adulthood of this patient, despite global negative selective pressure.[12 13] This phenomenon, though intriguing, would not be unexpected in human studies because leukocytes are usually utilised for genetic analyses. Rather, if the upid(AC)mat cells were barely present in leukocytes, they would not have been detected. It is likely, therefore, that upid(AC)mat cells have occupied a relatively large portion of the definitive haematopoietic tissues primarily as a stochastic event. Furthermore, parthenogenetic chimera mouse studies have revealed that parthenogenetic cells are found at a relatively high frequency in some tissues/organs including blood and are barely identified in other tissues/organs such as skeletal muscle and liver.[13] Such a possible tissue-specific selection in favour of the preservation of parthenogenetic cells in the definitive haematopoietic tissues may also be relevant to the predominance of the upid(AC)mat cells in leukocytes. In addition, a reduced growth potential of 45,X cells[14] may also have contributed to the skewed ratio of the two cell lineages.

Clinical features of this patient would be determined by several factors. They include: (1) the ratio of two cell lineages in various tissues/organs, (2) the number of imprinted regions or DMRs relevant to the development of specific imprinting disorders (eg, plural regions/DMRs on chromosomes 7 and 11 for SRS[9 10] and a single region/DMR on chromosome 15 for Prader–Willi syndrome (PWS)),[15] (3) the degree of clinical effects of dysregulated imprinted regions/DMRs (an (epi)dominant effect has been

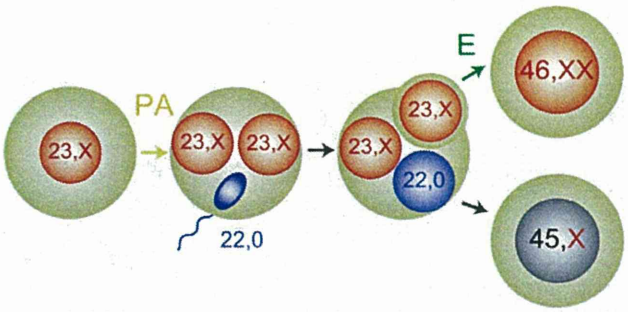

Figure 2 Schematic representation of the generation of the upid(AC)mat 46,XX cell lineage and the non-upd 45,X cell lineage. Polar bodies are not shown. PA, parthenogenetic activation; and E, endoreplication of one blastomere containing a female pronucleus.